

1 **Imbalance in the modern hydrologic budget of topographic**
2 **catchments along the western slope of the Andes (21–25°S):**
3 **Implications for groundwater recharge assessment**

4

5

6 ***** Provisionally accepted to Hydrogeology Journal – December 18, 2020 *****

7

8

9

10

11 David F. Boutt¹, Lilly G. Coenthel¹, Brendan J. Moran¹, LeeAnn Munk², Scott A. Hynek³,

12 ¹ Department of Geosciences, University of Massachusetts-Amherst, Amherst, MA, USA

13 ² Department of Geological Sciences, University of Alaska-Anchorage, Anchorage, AK, USA

14 ³Department of Geology and Geophysics, University of Utah, Salt Lake City, Utah USA

15

16

17

18

19 Mailing Address:

20

21 Department of Geosciences

22 611 North Pleasant Street

23 233 Morrill Science Center

24 University of Massachusetts

25 Amherst, MA 01003-9297

26

27

28

29

30 Key Points

- 31 ● Modern hydrologic budgets in topographic watersheds along the western margin of the
32 Andes (21–25°S) do not close.
- 33 ● Steady state regional flow from outside these basins yield large contributing areas of
34 conflicting nature.
- 35 ● Groundwater released from long-term storage is essential to balance modern water
36 budgets and impacts how water resources are managed.

37

38 **Keywords:** Salar de Atacama, Chile; recharge; regional groundwater flow; paleo-recharge;
39 pulsed recharge

40

41 Abstract

42 Modern rates of water discharge often exceed groundwater recharge in arid catchments.
43 This apparent mass imbalance within a catchment may be reconciled through either groundwater
44 flow between topographic drainages and/or the draining of stored groundwater recharged during
45 pluvial periods. We investigate discrepancies in the modern hydrologic budget of catchments
46 along the west flank of the Andes in northern Chile (21–25° S), focused on the endorheic Salar
47 de Atacama basin, and adjacent basins. We present uncertainty bounded estimates of modern
48 recharge rates that do not come close to balancing observed modern groundwater discharge
49 within topographic catchments. Two conceptualizations of hydrogeologic catchments
50 discharging to Salar de Atacama were explored with a simplified 2D groundwater model. Results
51 from models support the interpretation that subsurface interbasin flow and transient drainage of
52 groundwater from storage are required to balance water budgets along the plateau margin. The
53 models further examine whether this system is still responding to climatic forcing (on
54 paleoclimatic time scales) from pluvial periods and highlight general characteristics for similar
55 plateau margin systems including: (1) water level changes at the plateau margin are highly
56 sensitive to long-term (100–1000 yr) changes in recharge on the plateau, (2) extent and
57 magnitude of the changes in water table are controlled by the distribution of hydraulic
58 conductivity at the margin, and (3) the contributing area to the lower elevation catchment is itself
59 dynamic, and not coincident with the topographic boundary.

60 Plain Language Summary

61 Challenges remain in understanding the source of water to streams, springs, and wetlands
62 in the world's dry regions. This paper documents a discrepancy between the amount of water
63 entering a region compared to the amount of water leaving the system in the high desert of the
64 Chilean Andes. The amount of water leaving is shown to be greater than that entering the system
65 within the nearby drainage area. This is accomplished by combining physical estimates of
66 precipitation with chemical measurements of constituents in the local waters. We show that this
67 water is likely moving below ground across significant topographic barriers into the region.
68 However, this water is not enough to resolve the observed differences; therefore, we propose that
69 stored water within the region from wetter paleoclimatic conditions must be accounted for.
70 Together, these results have a significant bearing on how water is managed in the region and
71 elsewhere with similar climate and/or topography.

72 1. Introduction

73 Rates of anthropogenic water extraction and natural water discharge often exceed
74 groundwater recharge (e.g. safe yield or perennial yield) in arid catchments [e.g. *van Beek et al.*,
75 2011; *Gleeson et al.*, 2012]. Investigations of the closure of hydrologic budgets in topographic
76 catchments are the subject of many recent investigations [Schaller and Fan, 2009; Munoz et al.,
77 2016; Liu et al., 2020]. The analysis of Liu et al., (2020) suggests that 1 in 3 catchments
78 analyzed had an effective catchment area larger or smaller than the topographic catchment. This
79 mass imbalance within a catchment may be reconciled by subsurface interbasin flow between
80 topographic drainages and/or the draining of stored groundwater recharged during 500–1000 yr
81 before present pluvial periods. While these processes are well documented globally [e.g. *Alley et*
82 *al.*, 2002; *Gleeson et al.*, 2011; *Condon and Maxwell*, 2015], debates exist over methods to
83 physically and quantitatively distinguish between these mechanisms since both depend on
84 processes operating on large spatial and temporal scales difficult to directly observe [e.g. *Nelson*
85 *et al.*, 2004; *Masbruch et al.*, 2016; *Nelson and Mayo*, 2014]. The steady state hydrologic closure
86 assumption also underpins lake sediment-based paleo-precipitation reconstructions [e.g. *Urbano*
87 *et al.*, 2004, *Ibarra et al.*, 2018]. Therefore, we aim to better constrain the spatial and temporal
88 dimensions of subsurface interbasin flow and transient draining of groundwater storage at a site

89 where a modern hydrologic imbalance is documented in the topographic watershed. Both of
90 these issues are critical for understanding groundwater response to natural and anthropogenic
91 driven changes in aquifer recharge [Cuthbert et al., 2019].

92 Orogenic plateau margins, especially in arid regions, are characterized by steep gradients
93 in topography and climate that are conducive to the development of regional-scale groundwater
94 systems [Haitjema and Mitchell-Bruker, 2005; Gleeson et al., 2011] and mountain front recharge
95 sources. Closed basins may preserve geologic records of water fluxes over 10^2 – 10^6 year time
96 frames in the accumulation of evaporite minerals [e.g. Godfrey et al., 2003; Jordan et al., 2007;
97 Munk et al., 2018]. The Salar de Atacama hosts >1800 km³ of halite [Corenthal et al., 2016] in a
98 closed basin adjacent to the Altiplano-Puna plateau, and provides an extreme case to evaluate the
99 potential role of regional-scale groundwater flow and transient draining of groundwater storage
100 in sustaining water discharge rates over both modern and geologic timescales (Figure 1). Both
101 mechanisms invalidate the steady state topographic closure of the water budget, an assumption
102 often used for water resource management [e.g. as used by Dirección General de Aguas, 2013 in
103 the Salar de Atacama and documented in Gorelick and Zheng, 2015; Currell et al., 2016].

104 Sustaining the accumulation of massive (>1500 m thick [Jordan et al., 2007]) evaporites
105 in the basin necessitates maintaining the water table within several meters of land surface over a
106 5–10 million year time period [Tyler et al., 2006]. Estimates of recharge in the surface
107 topographic basins draining to the Salar de Atacama are not sufficient to balance the
108 evaporative/transpiration losses at the end of the flow system [Corenthal et al., 2016]. Individual
109 components of the water budget of the relatively small and hyperarid topographic watershed of
110 Salar de Atacama, and the adjacent Altiplano-Puna plateau [Kampf and Tyler, 2006; Salas et al.,
111 2010] have been studied extensively. While evidence for modern recharge in the central Andes
112 exists [Houston, 2002; Houston, 2007, 2009; Kikuchi and Ferré, 2016; Urrutia et al., 2019;
113 Viguier et al., 2018; Viguier et al., 2020;]; rates, spatial extent, and mechanisms are poorly
114 constrained [e.g. Montgomery et al., 2003; Jordan et al., 2015; Rissmann et al., 2015; Scheihing
115 et al., 2018; Viguier et al., 2020]. Halite accumulation, a proxy for long-term average water
116 inflow, confirms the observed hydrologic imbalance over geological timescales [up to 10 Myr;
117 Corenthal et al., 2016]. However, recently Munk et al. (2018) presented solute fluxes for the
118 surface and shallow sub-surface that account for halite and brine hosted solutes in the uppermost

119 (30 m) on a Myr timescale. Regional-scale groundwater flow, interbasin transfer, and pulsed
120 recharge events (10–100 year timescale) are documented [*Houston, 2006b; Rissmann et al.,*
121 *2015; Jordan et al., 2019*] in the region, and modern discharge in the Atacama Desert is
122 suggested to reflect the draining of groundwater recharged during episodic pluvial periods (10^3 –
123 10^4 year timescale) in the Late Pleistocene and Holocene [*Fritz et al., 1981; Herrera et al., 2021;*
124 *Sáez et al., 2016; Houston and Hart, 2004; Gayo et al., 2012*]. Recent work by Moran et al.
125 (2019) presents further evidence of the role of pre-modern groundwater dominating the discharge
126 of water to springs and lagoons while also showing that interbasin groundwater flow is
127 fundamental to explaining observations of discharge in the basin.

128 Previous efforts to balance the water budget of Salar de Atacama [*Rissmann et al., 2015;*
129 *Corenthal et al., 2016*], nearby closed basins [*Houston and Hart, 2004; Herrera et al., 2016*] and
130 plateau margins in general [e.g. *Andermann et al., 2012*] identified discrepancies in water flux
131 estimates, with water losses through evapotranspiration greatly exceeding modern watershed
132 inputs. Two mechanisms that have been previously considered to close the water budget
133 [*Corenthal et al., 2016 and Moran et al., 2019*]: (1) a larger watershed area that encompasses
134 regional-scale inter-basin groundwater flow paths recharged from precipitation at higher
135 elevations and (2) the modern hydrologic balance includes drainage of transient groundwater
136 storage recharged during wetter conditions are explored here. In this work, recharge from
137 precipitation is quantified by scaling point measurements to regional satellite datasets including
138 uncertainty, further defining the magnitude and time-scale of the hydrologic imbalance inferred
139 from observations of halite accumulation in Salar de Atacama [*Corenthal et al., 2016*]. Unique
140 datasets are integrated to (1) quantify the area of a regional-scale groundwater catchment
141 necessary to balance modern discharge, (2) approximate the role of late-Pleistocene recharge in
142 modern discharge, and (3) elucidate the mechanisms and physical processes by which water is
143 delivered to the basin. These data are then used to constrain a simplified 2D groundwater model
144 to solely understand the source of recharge to the basin floor. While the model is not focused on
145 the details of freshwater/brine interaction of the basin floor aquifer system, it does allow the
146 exploration of dynamic temporal and spatial scales of sources of recharge from both regional
147 groundwater flow and transient drainage in two hydrogeological conceptualizations. Together

148 these observations have significant bearing on modern and future water resource considerations
149 in arid regions.

150 2. Study Area

151 Salar de Atacama, a significant topographic depression with an area over 17,000 km²
152 adjacent to the Altiplano-Puna plateau of the Central Andes, serves as the focal point for our
153 analysis of the hydrologic imbalance in the region (Figure 1). The Salar de Atacama began
154 accumulating a massive halite deposit ~7 Ma, coincident with the uplift of the Central Andean
155 Plateau [*Jordan et al.*, 2002a, 2007; *Reutter et al.*, 2006]. The halite nucleus of the basin hosts a
156 lithium-rich brine that provides approximately one-third of the global lithium supply [*Maxwell*,
157 2014]. Alluvial fans are important hydrologic conduits to Salar de Atacama; supporting
158 numerous springs and seeps discharge in the transition zone around the halite nucleus, and
159 feeding environmentally sensitive wetlands and lagoons. The observed spatial trend of alluvium,
160 carbonate, gypsum, and halite downgradient along flow paths through the transition zone
161 documents the evaporation of inflow water until it reaches halite saturation [*Risacher et al.*,
162 2003]. Seven perennial and ephemeral streams emerge at stratigraphic and structural contacts but
163 lose all surface flow through alluvium before reaching gypsum and halite facies. These streams
164 act as important conduits for ephemeral and focused recharge of both local meteoric water and
165 regional groundwater emerging and re-infiltrating along its path (e.g. *Kikuchi and Ferré*, 2016;
166 *Scanlon et al.*, 2006). Shallow groundwater again emerges in complex lagoon systems above a
167 freshwater/brine interface near the salar margin [*Boutt et al.*, 2016; *Marazuela et al.*, 2019; *Munk*
168 *et al.*, *In Revision*]. A series of hydrogeologically important Plio-Pleistocene ignimbrites
169 originate from the Altiplano-Puna Volcanic Complex on the plateau [e.g. *Jordan et al.*, 2007;
170 *Salisbury et al.*, 2011] and extend into the Salar de Atacama subsurface; in the northern half of
171 the basin, these units are interpreted to be highly continuous. The north-south trending blind,
172 high-angle, down-to-the-east Salar Fault System accommodates over 1 km of offset through the
173 halite nucleus [*Lowenstein et al.*, 2003; *Jordan et al.*, 2007; *Rubilar et al.*, 2017; *Martínez et al.*,
174 2018]. *Jordan et al.* [2002] suggest that this fault acts as a barrier causing orogenic scale
175 groundwater flow paths to discharge in Salar de Atacama.

176 There are many studies that either explicitly document [*Montgomery et al.*, 2003;
177 *Rissmann et al.*, 2015; *Jayne et al.*, 2016] or imply [*Magaritz et al.*, 1990; *Pérez-Fodich et al.*,
178 2014; *Jordan et al.*, 2002a, 2002b] that water from the Andean Cordillera feeds downgradient
179 basins to the west via regional groundwater flow. In their analysis of the MNT aquifer (southeast
180 of Salar de Atacama), Rissmann et al. [2015] provide one of the few examples in the region
181 where hydrologic and geochemical information have been used to investigate and imply a
182 connection from a high elevation recharge area to discharge at the salar margin. The $^{87}\text{Sr}/^{86}\text{Sr}$
183 values for discharging water reported by Munk et al. [2018] support the possible link between
184 high elevation salt lakes and brines in Salar de Atacama proposed by Rissmann et al. [2015], and
185 are consistent with the observation of Grosjean et al. [1995] that many of the high elevation lakes
186 never reach Na-Cl saturation and that the water enriched in Na and Cl then drains to lower
187 elevation basins.

188 The Salar de Atacama basin, in the core of the Atacama Desert, is characterized by a
189 hyperarid to arid climate [*Hartley and Chong*, 2002]. Significant inter-annual precipitation
190 variability [*Garreaud et al.*, 2003] includes infrequent high-intensity rainfall events that produce
191 focused, ephemeral groundwater recharge [*Houston*, 2006b; *Boutt et al.*, 2016]. Because the
192 basin has been closed since at least the late Miocene [*Jordan et al.*, 2002a], surface water
193 discharge occurs only through evaporation. Sedimentary records suggest that variable arid to
194 hyperarid climates have dominated since 53 ka [*Bobst et al.*, 2001; *Godfrey et al.*, 2003], with at
195 least four periods wetter than the modern occurring since 106 ka [*Gayo et al.*, 2012]. Hydrologic
196 models for lakes in the Bolivian Altiplano similarly suggest that precipitation may have been 2–3
197 times more than the modern during these periods, with the most recent regionally wet periods
198 occurring during the late Pleistocene Tauca and Coipasa (Central Andean Pluvial Events)
199 [*Placzek et al.*, 2013]. Salar de Atacama sedimentary records further document variation in the
200 hydrologic balance of Salar de Atacama from >100 ka to present [*Bobst et al.*, 2001; *Godfrey et*
201 *al.*, 2003; *Lowenstein et al.*, 2003]. Records from paleo-wetland deposits south of Salar de
202 Atacama suggest less pronounced wet periods from 14–9.5 ka and 4–0.7 ka, [*Quade et al.*, 2008;
203 *Saez et al.*, 2016] consistent with vegetation records and other wetland deposits in the region
204 [*Betancourt et al.*, 2000; *Rech et al.*, 2002, 2003], as well as archeological records [*Gayo et al.*,
205 2012; *Santoro et al.*, 2017]. The climate around Salar de Atacama has been drier since the mid-

206 Holocene based on the water table being below ground surface at paleo-wetland sites and
 207 observations from sediment cores at Salar de Atacama [Rech et al., 2002; Quade et al., 2008;
 208 Placzek et al., 2013].

209 3. Study Approach and Methods

210 3.1 Conceptualization of the Modern Water Budget

211 Constraining the modern hydrologic budget is critical to evaluating whether the system is
 212 balanced within the topographic watershed. If the system is at steady state within the topographic
 213 watershed, groundwater recharge from precipitation (GW_{RCH}) plus surface water runoff (R)
 214 would balance all evapotranspiration (discharge) from Salar de Atacama (D_{SdA}) with no change
 215 in storage (S). When considering the water budget beyond the topographic watershed one must
 216 also consider an additional loss term of evapotranspiration from salars and lakes in high
 217 elevation closed basins ($D_{HighElevSalars}$). Diffuse discharge from precipitation in areas that are not
 218 salars is accounted for in the GW_{RCH} term.

219 The most conservative (more balanced) conceptualization of the modern hydrologic
 220 balance can be described by:

$$221 \quad \Delta S = GW_{RCH} + R - D_{SdA} - D_{HighElevSalars} \quad (1)$$

222 In the context of this equation, we provide uncertainty-bounded estimates of spatially distributed
 223 GW_{RCH} and $D_{HighElevSalars}$ throughout the region as the critically under-constrained term for
 224 assessing the hydrologic balance. A negative change in storage would suggest that water from
 225 outside the topographic basin or drawn from storage is needed to close the modern budget,
 226 whereas a positive change in storage would reflect recharge and surface water inputs currently
 227 outpacing evapotranspiration. We evaluate equation (1) for both the topographic watershed and
 228 the hydrogeologic watershed. We define the hydrogeologic watershed as the smallest potential
 229 contributing area within which the steady state hydrologic budget closes within reasonable
 230 uncertainty bounds (i.e. scenario M in Coenthall et al., [2016]). This conservative scenario has
 231 the potential to double count some discharge in both the GW_{RCH} and R terms since runoff is
 232 likely to be dominated by groundwater recharge.

233 A less conservative (less balanced) water budget conceptualization assumes that water in
234 spring-fed streams within the Salar de Atacama watershed is sourced entirely from groundwater.
235 In this conceptualization, precipitation events recharge aquifers (GW_{RCH}) but do not generate
236 runoff (R). This conceptualization of the modern hydrologic balance can be described by:

$$237 \quad \Delta S = GW_{RCH} - D_{SdA} - D_{HighElevSalars} \quad (2)$$

238 Equation 2 does not include a surface water runoff term (R) and therefore yields a more negative
239 estimate of the change in groundwater storage. A more negative change in storage would suggest
240 that even more water from outside the topographic watershed or drawn from storage is needed to
241 close the modern water budget. These equations and the following budgets do not consider
242 anthropogenic water extraction, because we are evaluating groundwater over geologic timescales
243 and rates are currently small compared to inflows reported here. Magnitudes of anthropogenic
244 freshwater pumping within the basin are on the order of $0.05 \text{ m}^3/\text{s}$ (Marazuela et al., 2019).

245 3.2 Precipitation

246 Precipitation estimates were obtained from the publicly-available Tropical Rainfall
247 Measurement Mission (TRMM) 2B31 dataset of Mean Annual Precipitation (MAP) derived
248 from 1–3 daily measurements at a resolution of 25 km^2 . A processed TRMM 2B31 dataset was
249 calibrated, validated, and provided by *Bookhagen and Strecker* [2008] over the period January 1,
250 1998, to December 31, 2009. This dataset was compared to gage measurements from 28
251 meteorological stations in the Region of Antofagasta maintained by the Chilean Dirección
252 General de Aguas (DGA) and one station on the salar maintained by the Sociedad Chilena de
253 Litio/Rockwood Lithium Inc./Albemarle (Figure S1 and S2). Power-law functions are fit to the
254 lower and upper bound of the DGA station-TRMM data (Figure S2) to provide constraints on
255 bias and uncertainty in the precipitation estimates. These bounds are used to estimate the median
256 (most plausible), lower and upper ranges of MAP in the region and to provide a range of possible
257 precipitation scenarios (Text S1). These ranges are incorporated in other dependent calculations
258 below.

259 3.3 Groundwater Recharge

260 To determine GW_{RCH} from precipitation (P), we apply the chloride mass balance (CMB)
261 method, which has been successfully applied to basins to the north and northwest of Salar de

262 Atacama [Houston, 2007, 2009], whereby

$$263 \quad GW_{RCH} = \frac{P \cdot Cl_p}{Cl_{gw} - Cl_{rw}} \quad (3)$$

264 Where:

265 Cl_p = chloride concentration in precipitation

266 Cl_{gw} = chloride concentration in groundwater

267 Cl_{rw} = chloride contribution to groundwater from rock weathering

268 Common assumptions used in the application of the CMB method include (1) precipitation (P) is
 269 the only source of chloride (Cl^-) to groundwater, and (2) Cl^- is conservative in the groundwater
 270 system [Bazuhair and Wood, 1996]. Table 1 presents analyses of precipitation samples and
 271 locations.

272 We apply CMB recharge rates ranging from 0.4–6 % (equation 3; Table 3) to selected
 273 low-elevation springs and wells using the median, lower, and upper TRMM 2B31 derived P
 274 estimates [Bookhagen and Strecker, 2008] to determine a range of potential GW_{RCH} rates. Given
 275 abundant chlorine (Cl) in volcanic glass (~0.1 weight %) and biotite (~0.2 weight %) from
 276 ignimbrites in the region, we allow (in the upper-end recharge scenario) for the potential that 50
 277 mg/l of Cl^- in groundwater could be sourced from rock weathering.

278 The basis for the GW_{RCH} estimates is data derived from over 600 water samples collected
 279 between 2011 and 2014. All samples were collected in clean HDPE bottles after passing through
 280 a 0.45 μm filter. Samples were shipped to the University of Alaska Anchorage where all
 281 chemical analyses were performed. Sample dilutions based on specific conductance were
 282 performed prior to analysis of Cl^- by ion chromatography. The isotopic composition of water
 283 samples (δ^2H , $\delta^{18}O$) was measured by a Picarro L-1102i WS-CRDS analyzer (Picarro,
 284 Sunnyvale, CA).

285 We select water samples for CMB calculations with stable isotopic composition of δ^2H
 286 and $\delta^{18}O$ close (deuterium excess of $< 5 \text{ ‰}$) to the global meteoric water line (Figure 2). There
 287 are 9 wells and 2 springs sampled 1 to 6 times within the SdA watershed and 6 wells sampled by
 288 Cervetto Sepulveda [2012] in the Chilean Puna Plateau that fit our criteria for CMB calculations
 289 (Sites shown in Figure 4b). Table 3 lists the details of the repeated sampling of each sample site
 290 and precipitation characteristics. These sites are located in areas of diffuse, mountain front, and
 291 ephemeral recharge zones and yield samples with stable isotopic compositions near the global

292 meteoric water line [Craig, 1961]. Each site is categorized into these 3 categories in Table 3
293 cover the range of potential recharge mechanisms in arid regions (Scanlon et al., 2006) and are
294 comprehensive assessments of potential recharge rates. These stable isotopic composition criteria
295 minimize the influence of evaporation and salt recycling known to occur in discharge zones. The
296 Cl^- concentration from multiple sampling events was averaged for each site. Measurements of Cl^-
297 in precipitation include 4 rain samples collected in SdA as part of this study (Figure 4b) and
298 published measurements from the Chilean Puna Plateau [Cervetto Sepulveda, 2012] and Turi and
299 Linzor region in the upper reaches of the Río Loa catchment [Houston, 2007, 2009].

300 A power function fit (Figure 3a) to the P and calculated GW_{RCH} is applied to the TRMM
301 2B31 datasets to generate lower, median, and upper estimates of the fraction of P that becomes
302 GW_{RCH} . Estimates of GW_{RCH} were confined to areas that do not contain permanent discharge
303 features (salars and lakes). The fraction of P that does not recharge groundwater is assumed to
304 evapotranspire or contribute to R. Herein, we pursue a conservative approach for closing the
305 water budget and consider that R is generated by precipitation runoff (equation 1).

306 3.4 *Evapotranspiration*

307 Evapotranspiration (D_{SdA}) estimates from the nucleus and transition zone of Salar de
308 Atacama are summarized from works that (1) coupled eddy covariance station measurements
309 taken in 2001 to remotely sensed land energy budgets (D_{SdA} range from 1.6–27.1 m^3/s) [Kampf
310 and Tyler, 2006] and (2) coupled lysimeter measurements collected from 1983–1985 to land-
311 type classifications from 1983–1985 (D_{SdA} of 5.6 m^3/s) [Mardones, 1986]. Additionally,
312 Marazuela et al. (2020a) presented estimates of evaporation from the salar with a value of 12.85
313 m^3/s . Of these values, we consider a maximum D_{SdA} of 22.7 m^3/s because higher estimates
314 significantly over-predict fluxes from the nucleus [Kampf and Tyler, 2006]. We consider a
315 minimum D_{SdA} of 5.6 m^3/s because it is the current estimate used to manage water resources of
316 the basin [Dirección General de Aguas, 2013]. The infiltration rate determined through the CMB
317 method is assumed to account for evaporation from anywhere not covered by a salar or lake.

318 Many closed basins above 3500 m in elevation host zones of focused evapotranspiration
319 ($D_{\text{HighElevSalars}}$). Because no reliable $D_{\text{HighElevSalars}}$ measurements were available, a linear regression
320 for potential ET (PET) (mm/year) as a function of ground elevation (m) for the Atacama region
321 was used (Text S2).

322 3.5 *Incorporation of Uncertainty in Hydrologic Balance Estimates*

323 Each component of the water balance contains uncertainty that propagates through the
324 calculations described above to consider a range of possible hydrologic balance estimates. At
325 each stage of the calculations, we consider these uncertainties and include them in final lower,
326 median, and upper-end recharge scenarios which are used to assess closure of the water budget.
327 The precipitation amounts from TRMM impact both the precipitation-recharge CMB functional
328 relationship (P in equation 3) as well as the assessed distributed recharge calculations.
329 Additionally, uncertainty in the chloride composition (Cl_p in Equation 3) of the precipitation also
330 impacts the effective recharge through the CMB calculation and functional relationship (equation
331 3). Our lower-end recharge estimates are calculated using the lowest possible precipitation
332 estimates (Figure S2 – Upper Curve), the lowest precipitation chloride concentration, and
333 omitting any Cl^- in groundwater sourced from rock weathering (Cl_{rw}). The median recharge
334 estimate is produced using the TRMM 2B31 directly with the average chloride concentration in
335 precipitation. Finally, the upper-end recharge estimates are calculated using the highest possible
336 precipitation estimates (Figure S2 – Lower Curve), the highest precipitation chloride
337 concentration, and the possibility of Cl^- sourced from rock weathering.

338 3.6 *Numerical Models of Plateau-Margin Hydrogeology*

339 A transient 2-dimensional groundwater model simulating the Altiplano-Puna plateau and
340 adjacent Salar de Atacama system was constructed using the MODFLOW finite difference code
341 for saturated flow [McDonald and Harbaugh, 1988]. The purpose of the model is to examine: (1)
342 the dynamic response times of a regional groundwater system to changes in groundwater
343 recharge that are of a magnitude similar to that predicted by paleoclimatic reconstructions
344 [Betancourt et al., 2000; Placzek et al., 2013]; (2) the sensitivity of water level responses to these
345 changes in groundwater recharge; and (3) whether the groundwater divide between water
346 draining to Salar de Atacama and water discharging to shallow basins on the plateau is dynamic
347 or static with respect to changing recharge. The framework for the model is based on previous
348 work in the Atacama by Houston and Hart [2004] and in the Murray Basin in Australia by
349 Urbano et al., [2004]. This model is not intended to be an exhaustive assessment of the
350 hydrogeologic conditions within the Salar de Atacama basin as compared to the work of
351 Marazuela et al., (2020b). We evaluate this model for two scenarios of hydraulic conductivity

352 that are designed to be conducive and restrictive to regional groundwater flow paths; the
353 conducive scenario is intended to approximate the northern half of Salar de Atacama with
354 continuous west dipping ignimbrites, and the restrictive scenario is intended to approximate the
355 southern half of Salar de Atacama where the Peine Block is present and ignimbrites are less
356 continuous. Together these scenarios represent the range of conditions expected along the
357 plateau margin (between the plateau and eastern side of the Salar). Initial hydraulic head
358 geometries were assigned based on the results of steady-state simulations, and the transient
359 models simulate a period of 100,000 years (using 100-year timesteps) immediately following a
360 step decrease in precipitation (recharge).

361 The model domain is 240 km long (active domain of 219,200 m), unit width, and 3,000 m
362 thick with grid dimensions of 200 m x 1 m x 200 m in the upper 7 layers and 200 m x 1 m x 400
363 m in the lower 4 layers. Elevations of the top grid cells were interpolated from a smoothed
364 ASTER GDEM. The bottom of the model is a no-flow boundary. **The right hand boundary is set**
365 **to a major divide (no flow) of the Andean plateau and given the climatic gradient across this**
366 **region, the distribution of recharge is likely to create a strong divide at this location. The effect**
367 **of this boundary is justified because of the small changes in simulate heads. The left hand**
368 **boundary is also a no-flow boundary condition of the Salar de Atacama.** On the top boundary,
369 there are 207 constant head cells in the upper layer at an elevation of 2300 m asl, representing
370 the Salar de Atacama surface. Specified flux boundaries were assigned to all other top cells.
371 There are 119 drains along the plateau with a conductance of 1,000 m²/day. Along the plateau at
372 an elevation of 3,893 masl, 28 drains were assigned an elevation of 3,993 masl and conductance
373 of 10 m²/day for the steady state run to produce a high elevation lake similar to those described
374 by *Grosjean et al.* [1995], *Condom et al.*, [2004] and others. For the transient runs, the drains
375 were assigned an elevation of 3,893m (top cell elevation) and conductance of 1,000 m²/day to
376 simulate a salar. Recharge was assigned to any top cell that was not already a drain or constant
377 head boundary. For the initial steady-state simulations, recharge was determined by multiplying
378 the TRMM 2B31 precipitation raster by a factor of three and applying equation 4 to this
379 precipitation raster. This multiplication factor represents the upper estimates of precipitation
380 during past pluvial periods in the most recent 130 ka [*Placzek et al.*, 2013]; and thus the most
381 conservative conceptualization of the water budget. This resultant raster was then interpolated to

382 the model grid. For the transient run, modern GW_{RCH} rates were determined by applying
383 equation 4 for GW_{RCH} to the modern TRMM 2B31 dataset and interpolating the resultant raster
384 to the model grid. Interpolating the 3x modern precipitation and modern precipitation estimates
385 for recharge inputs to the model captures the spatial distribution of GW_{RCH} across the plateau as
386 well as the predicted relative magnitude of paleo- to modern- GW_{RCH} from the late Pleistocene to
387 present based on *Betancourt et al.* [2000] and *Placzek et al.* [2013]. There are no other hydraulic
388 sources or sinks in the model and the 2D model does not account for flow transverse to the
389 domain, surface water features, or direct precipitation runoff.

390 Two heterogeneous, isotropic hydraulic conductivity distributions were examined based
391 on a geologic cross-section through the Salar de Atacama basin and the western Altiplano-Puna
392 plateau by *Reutter et al.* [2006] (Figure 1; Figure 6). These scenarios are designed to represent:
393 (1) southeastern Salar de Atacama characterized by an uplifted, low permeability block of
394 Precambrian to Carboniferous basement that interrupts the plateau margin (restrictive to regional
395 flow) and (2) northeastern Salar de Atacama characterized by monoclinal folding of laterally
396 extensive ignimbrites (conducive to regional flow). Hydraulic conductivities for the geologic
397 units described in *Reutter et al.* [2006] were assigned based on standard values from *Ingebritsen*
398 *and Manning* [1999] and range from 0.01 to 10 m/day. For the transient simulations, a confined
399 specific storage of 10^{-4} was assigned uniformly to the entire domain. The choice of a single value
400 of storage allows the exploration of the sensitivity of the model results to hydraulic conductivity.

401

402 4. Results

403 4.1 Assessment of the Hydrologic Balance and Uncertainty

404 On the Salar de Atacama salt flat annual precipitation averages 16 mm/year [*Sociedad*
405 *Chilena de Litio Ltda.*, 2009], whereas >300 mm/year [*Bookhagen and Strecker*, 2008; *Quade et*
406 *al.*, 2008] may occur above 5,000 m within the topographic watershed (Figure 1, Figure 3b).
407 Approximately 50–80 mm/year of snow water equivalent occurs at 4500 m asl [*Vuille and*
408 *Ammann*, 1997] but the majority likely sublimates before infiltrating [*Johnson et al.*, 2010;
409 *Dirección General de Aguas*, 2013]. Based on the TRMM 2B31 dataset mean annual
410 precipitation from 1998 to 2009, including the wetter than average 2001/2002, is $30.7 \text{ m}^3/\text{s}$ (23.4

411 for lower bound and 51.7 m³/s for upper bound) in recharge zones in the topographic watershed
412 (Table 2), equivalent to a mean of 48 mm/year with a range of 0–340 mm/year (standard
413 deviation of 45 mm/year). For the median precipitation scenario, only 7% of the watershed area
414 receives more than the 120 mm/year of precipitation threshold required for significant GW_{RCH}
415 [Scanlon *et al.*, 2006; Houston, 2009] (Figure 3, Figure 4a), and most precipitation occurs above
416 3,500 m. Using this (median) scenario, infiltration rates of nearly 100% throughout the
417 topographic watershed would be required to balance the highest estimates of D_{SdA}.

418 Chloride concentration in precipitation samples ranged from 5–16 mg/L (Table 1). We
419 combine our CMB results with those from the Turi and Linzor basins [Houston, 2007, 2009] to
420 establish a new relationship for GW_{RCH} as a function of P (Figure 3) in this region. The upper
421 end of our fit is roughly parallel to the equation of [Houston, 2009]. The range of chloride
422 concentrations in precipitation bounds does not impact the fit of this function to the data,
423 therefore we use a single relationship between precipitation and recharge (Text S3 and Figure
424 S5). This relationship is fit using a power law with an R² of 0.82 as described:

$$425 \quad \text{GW}_{\text{RCH}} = (1.3 \cdot 10^{-4}) \cdot P^{2.3} \quad (4)$$

426 Applying equation (4) to the median TRMM 2B31 dataset predicts 1.1 m³/s (1.1 for lower bound
427 and 2.1 m³/s for upper bound) of recharge within the topographic watershed (Figure 4b, Table 2),
428 with infiltration rates ranging from 0.5–3.5% based on a precipitation Cl⁻ concentration of 8
429 mg/l, or 0.3–9.0% considering a range of precipitation Cl⁻ concentrations from 5–16 mg/l (Table
430 3, Figure 3). Similar to arid regions globally [Scanlon *et al.*, 2006] and the Central Andes
431 [Houston, 2007], significant (>0.1 mm/yr) GW_{RCH} only occurs when precipitation exceeds 120
432 mm/year. This approach stands in contrast to other work in the basin [e.g. Marazuela *et al.*,
433 2019] that forces steady-state closure in the hydrologic budget using extremely high infiltration
434 rates of 35–85%. The extreme values of mean infiltration (compared to global data in Scanlon *et al.*,
435 2006) are solely supported by the hydrological assumption that the water budget is balanced
436 within the topographic watershed.

437 Estimates of D_{SdA} range from 5.6–13.4 m³/s [Mardones, 1986; Kampf and Tyler, 2006]
438 (Table 2). We use a range of D_{SdA} estimates in our calculations, considering a minimum of 9.5
439 m³/s based on the spatially variable latent heat flux method [Kampf and Tyler, 2006] and

440 lysimeter study [Mardones, 1986]. We predict that $D_{\text{HighElevSalars}}$ in the hydrogeologic watershed
441 totals $5.0 \text{ m}^3/\text{s}$ (uncertainty range of $1.8\text{--}17.8 \text{ m}^3/\text{s}$) (Figure 4c, Table 2).

442 Approximately $3.19 \text{ m}^3/\text{s}$ of shallow subsurface groundwater enters Salar de Atacama as
443 calculated by Corenthal et al. (2016) and Munk et al., (2018). The *Direccion General de Aguas*
444 (2013) estimates total streamflow to Salar de Atacama is $1.58 \text{ m}^3/\text{s}$ based on gage measurements,
445 which alone matches our new range of estimates of GW_{RCH} within the topographic watershed
446 ($1.1\text{--}2.1 \text{ m}^3/\text{s}$). The sum of this shallow groundwater and streamflow ($4.77 \text{ m}^3/\text{s}$) is consistent
447 with but smaller than prior low estimates of D_{SdA} ($5.6 \text{ m}^3/\text{s}$); however, GW_{RCH} within the
448 topographic watershed accounts for only 24% of these inflows and only 5–20% of D_{SdA} . To
449 balance the full range of discharge from evapotranspiration (5.6 to $13.4 \text{ m}^3/\text{s}$) with GW_{RCH} (1.1 –
450 $2.1 \text{ m}^3/\text{s}$) in the Salar de Atacama topographic watershed, a watershed average infiltration rate of
451 21 to 86 % is required. Such rates greatly exceed average infiltration rates of 0.1–5% for arid
452 regions globally [Scanlon et al., 2006], as well as infiltration rates observed in the nearby Linzor
453 and Turi basins [Houston, 2007, 2009].

454 Within the topographic watershed, D_{SdA} is 2–8 times ($5.6\text{--}13.4 \text{ m}^3/\text{s}$) higher than the
455 combined inputs of modern recharge from precipitation and streamflow (Figure 5; Table 2).
456 Some streamflow is likely sourced from groundwater [e.g. Hoke et al., 2004] and therefore
457 counted twice, yielding more conservative estimates of hydrologic imbalance. The
458 hydrogeologic watershed required for $\text{GW}_{\text{RCH}+\text{R}}$ to balance evapotranspiration for our estimated
459 range of recharge values has a surface area over $75,000 \text{ km}^2$, 4 times larger than the topographic
460 watershed (Figure 5 scenario M). Even the high estimates of $\text{GW}_{\text{RCH}+\text{R}}$ fail to explain the low
461 estimates of D_{SdA} for watersheds A through I.

462

463 4.2 *Numerical Simulations of a Plateau Margin Groundwater System*

464 Numerical simulations of water level response to changes in plateau long-term recharge
465 conditions show strong spatial variability with the most sensitivity observed in the area of the
466 western and eastern plateau margins (Figure 7). Water levels have a greater magnitude of
467 response to recharge in the “restrictive to” than in the “conductive to” regional flow simulations;
468 however, the pattern of head decline was consistent between the models. In both simulations,
469 less than 10 m of change in head was observed in cells within 7 km of a constant head cell at

470 Salar de Atacama throughout the 100,000-year simulation. The maximum head decline occurred
471 near observation points 15 and 16, reaching 845 m of decline in the restrictive simulation and
472 370 m of decline in the conducive simulation. The magnitude of head decline increased with
473 increasing elevation along the plateau margin. From west to east across the plateau, the
474 magnitude of head decline decreased, reaching a minimum of 100 m decline near the high
475 elevation drain cells for both simulations.

476 Figure 8 presents a comparison between modern (observed) and simulated hydraulic
477 head observations in the conducive and restrictive cases. Observation points (see actual locations
478 on Figure 5 and projected locations in Figure 7) are placed approximately at model locations
479 with corresponding modern and paleo- water table elevation estimates (Table S6). The two
480 models are conceptual, and not specifically developed to match field observations; nonetheless,
481 comparing results from the two models with field observations supports general interpretations
482 and places first-order constraints on the permeability structure of the plateau and plateau margin.

483 The pattern of modeled head declines is consistent with observed patterns inferred from
484 paleoclimatic studies. During the Central Andean Pluvial Event in the late Pleistocene and early
485 Holocene, paleowetland deposits and river incision records at elevations <3500 m show water
486 table fluctuations on the scale of 1–25 m [e.g. *Betancourt et al.*, 2000; *Rech et al.*, 2002; *Quade*
487 *et al.*, 2008], while lake levels and core records on the Altiplano-Puna plateau at elevations
488 >3500 m show water table fluctuations of up to 130 m [*Grosjean et al.*, 1995; *Placzek et al.*,
489 2006, 2013]. In both modeled scenarios, after 10,000 years, the water table on the plateau margin
490 at elevations <2,600 m declined by <25 m. The water table on the plateau near the discharge
491 zone at elevations between 3880 m and 4120 m declined approximately 100 m by 10,000 years.
492 No field observations of changes in the water table are available on the plateau in areas distal to
493 discharge zones.

494 — The ratio of flow out of the model from constant head cells on the salar surface and
495 drains on the plateau margin (D_{SdA}) to total domain model recharge ($\text{GW}_{\text{TotalRCH}}$) is used as a
496 metric to evaluate changes in the flow budget of the model over time. For all time steps of the
497 100,000-year transient simulation, GW_{RCH} was assigned modern values. This ratio is plotted as a
498 function of simulation time in Figure 9. If the ratio of D_{SdA} to $\text{GW}_{\text{TotalRCH}}$ is greater than 1, then
499 D_{SdA} must be supported in part by draining groundwater storage because the volume of water

500 entering the salar exceeds the total model recharge, where the fraction of discharging water
501 supplied by draining storage is described by $(D_{SdA} - GW_{TotalRCH})/D_{SdA}$. If $D_{SdA}/GW_{TotalRCH}$ equals
502 1, then D_{SdA} is entirely balanced by $GW_{TotalRCH}$ in the model domain, and no $GW_{TotalRCH}$ is
503 discharging on the plateau. If $D_{SdA}/GW_{TotalRCH}$ is less than 1, then D_{SdA} is less than $GW_{TotalRCH}$ in
504 the model domain and some fraction of $GW_{TotalRCH}$ is discharging from drains on the plateau
505 ($D_{HIGHLEV}$).

506 For the restrictive to regional groundwater flow simulation, 60% of D_{SdA} is sourced from
507 draining storage at $t=100$ years, and D_{SdA} is supplied entirely by $GW_{TotalRCH}$ after 19,200 years.
508 For the conducive to regional groundwater flow simulation, 70% of D_{SdA} is sourced from
509 draining storage at $t=100$ years, and D_{SdA} is supplied entirely by $GW_{TotalRCH}$ after 37,600 years.
510 In the “conductive” simulation the water table on the plateau lies below the ground surface
511 elevation and thus the elevation of the drains. For the “restrictive” simulation, $D_{SdA}/GW_{TotalRCH}$ is
512 less than 1 for all times greater than 19,200 years. These results suggest that the low permeability
513 zones must be present between the plateau and the basin floor to allow the high-elevation lakes
514 and salars to exist.

515 If the change in $D_{SdA}/GW_{TotalRCH}$ between each time step is small, then the model has
516 approached a steady state and the modeled system is adjusted to a reduction in groundwater
517 recharge from 3x modern to modern. For the restrictive simulation, the dynamic response time is
518 approximately 85,000 years and approximately 38,000 years for the conducive simulation. These
519 results are consistent with the dynamic response time calculations using general bulk aquifer
520 properties of 42 kyr (Text S5) for the hydrogeologic watershed. The model results do not support
521 the modern steady-state budget for systems with long response times.

522 ___Model results support interpretations that the groundwater divide separating water
523 flowing to Salar de Atacama and water discharging within the plateau does not coincide with
524 topographic watershed boundaries (Figure 7 – vertical lines). In the initial steady state
525 simulations for both scenarios, the groundwater divide occurs approximately 100 km from the
526 easternmost constant head cell at Salar de Atacama (or 50–70 km from the topographic divide).
527 This length scale defines the upper distribution of flow paths discharging at Salar de Atacama.
528 Once the transient simulation begins, the groundwater divide moves westward closer towards
529 Salar de Atacama as water is released from storage to augment discharge at Salar de Atacama. In

530 both simulations, after approximately 1,000 years, the groundwater divide reverses direction and
531 begins to migrate eastward away from Salar de Atacama as the volume of water released from
532 storage decreases, and regional groundwater recharge is captured. In the restrictive simulation,
533 the position of the groundwater divide stabilizes by approximately 50,000–100,000 years around
534 130 km east of the easternmost constant head cell of Salar de Atacama. In the conducive
535 simulation, the groundwater divide reaches the easternmost boundary of the model after 9,000
536 years and does not move westward for the remainder of the simulation.

537 These results demonstrate that the groundwater divide of the plateau-margin system is
538 dynamic at time scales of 1 kyr similar to observed changes in climate and moves in response to
539 changing recharge conditions. The position of the divide is also sensitive to the presence of a
540 lower conductivity block separating the discharge zone from the plateau, especially over longer
541 time periods. While the “restrictive” case shows the greatest head change, it should be expected
542 that groundwater divides along such portions of the plateau margin will be more stable over time
543 than other segments of the plateau margin. This simple model lacks the more complex physics of
544 other published models in the region and the Salar de Atacama basin [Jayne et al., 2016;
545 Marazuela et al., 2020b]. With the focus on understanding recharge zone hydrogeology, this
546 model does not simulate density-driven flow that is needed for resolving salar margin flow
547 patterns and processes [Marazuela et al., 2018; McKnight et al., In Revision]. Nor does this
548 model incorporate thermo-haline dependent flow as we are primarily interested in water table
549 response to changing recharge flux. Ultimately, this model represents a sensitivity analysis
550 exploring the changing recharge conditions in the recharge area of regional flow systems to
551 endorheic basins.

552 **5. Discussion and Conclusions**

553 The persistence and scope of questions relating to water imbalance in the Atacama Desert
554 [e.g. *Magaritz et al.*, 1990; *Houston and Hart*, 2004; *Jordan et al.*, 2015], which is subject to
555 high water resource demand for mining purposes, highlights the importance of better
556 constraining groundwater divides and groundwater storage in these modern and paleo hydrologic
557 systems. Observations of discharge along the Altiplano-Puna plateau margin exceed our
558 estimates of modern recharge rates to groundwater aquifers. In the absence of substantial

559 overland flow, this leaves an extreme hydrologic imbalance for catchments along the plateau
560 margin.

561 The modern hydrologic balance of the Salar de Atacama topographic watershed does not
562 close within reasonable uncertainty bounds (Table 2; Figure 5). The arid climate, high
563 topographic relief, and presence of laterally continuous permeable volcanic units dipping
564 towards Salar de Atacama support the potential for regional groundwater flow paths [Tóth, 1963;
565 *Haitjema and Mitchell-Bruker*, 2005]. Within the proposed hydrogeologic watershed of 75,900
566 km² (Table 2; Figure 5 scenario M), $\text{GW}_{\text{RCH}} + \text{R}$ balance evapotranspiration ($\text{D}_{\text{SDA}} +$
567 $\text{D}_{\text{HighElevSalars}}$) while maintaining an overall topographic gradient driving groundwater flow
568 towards Salar de Atacama; however, this watershed delineation is non-unique. Proposed
569 recharge areas for many adjacent watersheds along the western Altiplano-Puna plateau margin
570 overlap (Figure 5). We propose that regional groundwater flow does play an important role in the
571 modern hydrologic balance of Salar de Atacama; however, fossil groundwater likely also plays a
572 role in this discrepancy.

573 Inter-basin groundwater flow is assumed to occur in the central Andes [*Anderson et al.*,
574 2002; *Jordan et al.*, 2015], including the MNT aquifer that discharges in the southern Salar de
575 Atacama [*Rissmann et al.*, 2015]. To explain the existence of giant nitrate deposits in the Central
576 Depression southwest and northwest of Salar de Atacama, *Pérez-Fodich et al.* [2014] also
577 suggest regional groundwater flow paths. To the north, interbasin groundwater flow is also
578 necessary to close the hydrologic budget of the Río Loa catchment (drainage area = 33,570 km²);
579 where the Chilean DGA estimates a total of 6.4 m³/s of water discharge [*Jordan et al.*, 2015], but
580 we calculate only 1.6 – 4.0 m³/s of GW_{RCH} within that topographic watershed. Using the
581 plausible groundwater system of the Río Loa proposed by *Jordan et al.* [2015] (Figure 5); we
582 estimate that approximately 8.5–14.3 m³/s of GW_{RCH} occurs within this zone; however, this
583 boundary overlaps with the major discharge zone of the Salar de Uyuni as well as a significant
584 portion of a potential hydrogeologic watershed for Salar de Atacama. For these adjacent
585 watersheds to have distinct recharge zones and be hydrologically balanced, it is required that
586 some water must be drawn from transient storage.

587 Transient draining of groundwater storage may be able to reconcile the budgets.
588 We calculate the mean residence time of water [*Gelhar and Wilson*, 1974; *Lasaga and Berner*,

589 1998] within the Salar de Atacama watershed to be 4.9 kyr using the conservative D_{SDA} rate of
590 $5.6 \text{ m}^3/\text{s}$, an active aquifer thickness of 500 m, an area of $17,257 \text{ km}^2$ (i.e. area of the topographic
591 watershed), and an effective porosity of 0.25. The dynamic response time [Houston and Hart,
592 2004] for the topographic watershed is 9.2 kyr and 42 kyr for the hydrogeologic watershed (Text
593 S4). In systems with long residence and response times, the assumption that modern recharge
594 rates must balance discharge rates is invalidated by having equilibration times greater than the
595 timescale of documented climatic changes [Currell et al., 2016]. High and low elevation
596 groundwater age estimates lack a significant component of modern recharge further suggesting
597 that these systems respond over long time scales [Houston, 2006b; Moran et al, 2019].
598 Evaporation at the smaller Salar de Veronica located 50 km southwest of Salar de Atacama
599 exceeds modern recharge, and this imbalance has been explained by residual hydraulic head
600 decay (i.e. groundwater storage) due to episodic recharge [Houston and Hart, 2004].

601 Some workers who have assessed the Salar de Atacama hydrological system have done
602 so under the basic assumption that the water budget can be closed within its topographic
603 watershed on modern timescales [Marazuela et al., 2019]. We argue that for several reasons this
604 is a fundamentally flawed and unfounded assumption. As recent work has shown [Corenthal et
605 al., 2016; Moran et al., 2019], this assumption is inadequate to assess large, high relief, arid or
606 semi-arid systems such as the Salar de Atacama. Conceptual models based on these assumptions
607 have required unrealistic estimates of diffuse recharge (35–85%) to balance water budgets, rates
608 that exceed any established estimates in arid or semi-arid areas by more than an order of
609 magnitude [e.g. Scanlon et al., 2006; Houston, 2009] and are not supported by any hydrological
610 field evidence. Figure 10 presents a summary of recharge rates across northern Chilean
611 catchments and the global compilation (including results reported here). It is clear that the
612 studies that balance water/energy budgets on the topographic basins (in blue) result in much
613 larger effective recharge rates and in one case [Marazuela et al., 2019] report some of the highest
614 recharge rates in the published literature.

615 An argument used to justify the assumption of water budget closure on modern
616 timescales is that the absence of a strong evaporation signal in groundwater recharge precludes
617 groundwater recharge sourced outside the watershed or from the plateau [Marazuela et al.,
618 2019]. Isotopic composition of water can be presented as evidence that groundwater has not

619 undergone evaporation and closely reflects modern meteoric inputs. This reasoning is
620 incomplete and does not invalidate a larger recharge area or draining of groundwater from
621 storage. The lack of a strong evaporative fractionation signal (as would result from open-water
622 evaporation) does not by itself indicate modern meteoric water is infiltrating quickly.
623 Fractionation from soil water losses is commonly observed in arid areas but results in small
624 fractionation effects on the bulk isotopic composition of recharge water compared to open-water
625 evaporation [Barnes & Allison, 1988; DePaolo et al., 2004; Sprenger et al., 2015]. Though some
626 fractionation of recharge derived from snowmelt likely occurs (through sublimation and
627 evaporation), the lack of permanent or deep seasonal snowfields, the dominance of summer
628 precipitation [Vuille & Ammann, 1997] and substantial loss of water volume available for
629 recharge from sublimation [Stigter et al., 2018] likely mean this signal is quite small relative to
630 an open-water evaporation signal [Beria et al., 2018]. In the most comprehensive analysis of
631 water isotope data in this basin, Moran et al., 2019 show that inflow waters have a consistent d-
632 excess signature aligning parallel to but below the LMWL. It is proposed that this signal is the
633 result of small net evaporative enrichment effects on recharge water combined with the
634 fingerprint of pluvial period groundwater recharge now draining from storage and/or
635 fractionation from thermal water-rock interaction. This d-excess signal has been observed by
636 others in this region and similar environments [Fritz et al., 1981; Magaritz et al., 1989; Aravena,
637 1995; Meijer & Kwicklis, 2000] and Scheihing et al. (2018) suggests that it is the result of
638 evaporative processes alone. But the relatively small magnitude of the offset (lc-excess of -10‰
639 to -20‰), its slope (very similar to the LMWL), and the lack of an enriched endmember of
640 recharge waters required to produce the signal observed in SdA discharge suggests this signal is
641 likely the net result of multiple processes. Together with their analysis of ^3H in waters Moran et
642 al., 2019 demonstrate that recharge likely occurs primarily at the highest elevations and flows to
643 the basin over 10^2 – 10^4 year time scales. A system operating on these time scales will integrate
644 various degrees of transience from the many climatic variations which have occurred over this
645 time frame and further invalidate any steady state assumptions of water balance. Without robust
646 evidence for these very high recharge rates or integration of them over a long temporal scale,
647 conceptual models based on a closed steady state system and models calibrated based on these
648 assumptions are not scientifically defensible or reasonable

649 The steady state assumption that modern recharge equals discharge within the
650 topographic catchment is clearly not appropriate in this setting, despite its prevalence in the
651 watershed management approaches throughout the region and globally. Global assessments of
652 catchment water budgets [Liu et al., 2020] have documented extensive discrepancies between
653 topographic watersheds and surrounding catchments. In order for recharge to equal discharge
654 with hydrologic closure at steady state conditions, groundwater infiltration rates must be
655 unrealistically high (21–86%; cf. *Scanlon et al.*, [2006]). Recharge rates in basins to the east
656 (Tuyajto; *Herrera, et al.* [2016]) and north (e.g. Pampa del Tamarugal; *Jayne et al.*, [2016]; and
657 Salar de Huasco; *Uribe et al.*, [2016]) using steady-state conditions are fundamentally flawed in
658 the conceptualization of the sources of recharge water. The implications of these assumptions
659 have the possibility of over-allocating water to users, resulting in significant environmental
660 impacts and social injustice. Recharge during infrequent and sporadic precipitation events
661 [Houston, 2002; Kikuchi and Ferré, 2016; *Boutt, et al.*, 2016; *Masbruch et al.*, 2016] could be a
662 potential source of water but it must be explained in the context of recharge rates constrained
663 using CMB estimates from diffuse and ephemeral sources, which are argued to reflect long-term
664 average recharge rates.

665 The conclusion that recharge water is moving from up-gradient closed basins requires a
666 reconceptualization of how topographic boundaries are treated in catchment hydrologic budgets
667 as widely applied elsewhere [*Haitjema and Mitchell-Bruker*, 2005; *Gleeson et al.*, 2011]. Effort
668 should be spent on identifying the hydrogeologic controls on the flow paths of water and being
669 able to distinguish this regional groundwater from local groundwater inputs using elemental,
670 isotopic, and molecular tracers [e.g. *Moran et al.*, 2019]. In the case of regional steady state flow
671 toward such basins that are groundwater importers, shallow hydraulic heads should show strong
672 downward gradients and hydraulic heads lower in magnitude towards the discharging basin.
673 Both of these conditions have significant implications for the water budget of the high elevation
674 (> 4000 m) closed basins on the plateau. The water budget of these basins should be negative
675 with some fraction of water flowing out of the basin to neighboring basins. One nearby basin,
676 Laguna Tuayito shows that this is the case [*Herrera et al.*, 2016]. Secondly, water levels in these
677 basin floors are likely perched above a regional groundwater table. Both considerations have
678 strong implications for lake-based precipitation paleo-climate reconstruction. Reconstructions

679 assume that lake levels in the closed basin respond solely to precipitation minus evaporation. If
680 one were to assume losses of water between basins or out the basin bottom to the regional
681 groundwater table, it would lead to an underestimation of precipitation in the region. Basins that
682 receive substantial groundwater input from another would lead to an overestimate of
683 precipitation. Understanding the magnitude of hydraulic losses through infiltration from perched
684 basins above a regional water table is critical.

685 By coupling solute and water budgets, additional constraints may be gained. *Corenthal et*
686 *al.* [2016] demonstrated that the modern sodium (Na) flux to the Salar de Atacama basin could
687 account for the halite and brine deposits over ~10 Ma, consistent with geological constraints. If
688 the Na concentration of inflow water is assumed to be constant over this interval, the long-term
689 average discharge rates are also required to remain relatively constant. Both the water molecule
690 and any conservative solutes must achieve mass balance in a realistic conceptualization of the
691 hydrologic system. Therefore, agreement in water and solute budgets is strong support for a
692 realistic and reasonable hydrologic model. Similarly, the recharge area and transient storage can
693 be constrained by solute budgets. Although this is outside the scope of this manuscript, we
694 suggest that the yield of weathering derived solutes per unit area must fall within the range
695 observed for arid montane catchments globally to justify the size of the hydrogeologic
696 watershed. Additionally, solute release rates from groundwater systems must match the modeled
697 draining of transient storage and predicted mean residence times for groundwater. In the case
698 where such constraints cannot be reconciled, a reconceptualization of the hydrogeologic model
699 will require adjustments that affect any combination of the following: (1) the scale of regional
700 groundwater flow, (2) the mean residence time of water, and (3) the potential for deep, under-
701 sampled flow paths. We argue that any reasonable assessment of the water balance of basins
702 such as these requires consideration of both the water and solute budgets.

703 These regional flow and transient storage mechanisms are inferred to account for the
704 majority of the missing water flux; however, additional flow paths (e.g. orogenic water) and
705 systematic errors in ET and/or GW_{RCH} estimates could also explain portions of the imbalance.
706 Infrequent, high-intensity precipitation events are known to rapidly recharge the groundwater
707 system in areas where the water table is near the surface [*Boutt et al.*, 2016]. For the brine budget
708 of Salar de Atacama, such events are important to balance discharge from pumping and the low

709 ET rates (<0.1 mm/year) in the halite aquifer. The potential for higher recharge rates in salars
710 during intense rainfall is not included in the budget calculations. Nonetheless, the CMB method
711 integrates over long-term timescales of different types of recharge and accounts for these events
712 in alluvium elsewhere in the Atacama [*Bazuhair and Wood, 1996; Houston, 2006b*]. Therefore,
713 the CMB approach does account for different types (diffuse, ephemeral, focused) of freshwater
714 recharge mechanisms.

715 Our present conceptualization of the extreme modern hydrologic imbalance along the
716 western margin of the Altiplano-Puna plateau can be explained by a combination of regional
717 groundwater flow and transient draining of groundwater storage. The transient draining of
718 groundwater storage is a required component of any water budget because presumed recharge
719 areas for many watersheds at the plateau margin overlap. Dynamic groundwater flow modeling
720 suggests: (1) the water level changes at the salar margins (and discharging water to basin floors)
721 are highly sensitive to changes in recharge on the plateau, (2) the extent and magnitude of the
722 changes in hydraulic head are controlled by the distribution of hydraulic conductivity at the
723 plateau margin, (3) the contributing area to Salar de Atacama changes, is not coincident with the
724 topographic boundary, and is a dynamic feature, and (4) it is difficult to reconcile the modern
725 position of the “water table” on the plateau with the regional groundwater flow conceptualization
726 and the modern discharge to Salar de Atacama (i.e., modern salars are perched and lose water to
727 surrounding basins and ultimately to Salar de Atacama and adjacent plateau margin catchments).

728 The hydrologic imbalance at Salar de Atacama has important implications for paleoclimatic
729 reconstructions because the imbalance implies that paleo-lake catchments on the Altiplano lost
730 water to Salar de Atacama altering their hydrologic budgets and further complicating lake-level
731 based paleoclimatic reconstructions. Because water resources of Salar de Atacama (and other
732 basins worldwide) are managed under the steady state assumption, these findings have
733 implications for efforts to sustainably allocate water resources for mining, agricultural and
734 environmental interests. Such considerations apply to many continental settings with strong
735 gradients in landscape and climate, though the margins of the large orogenic plateau are likely to
736 exhibit the greatest hydrologic imbalance by virtue of their scale.

737 **6. Acknowledgments**

738

739 The authors would like to acknowledge Rockwood Lithium, Inc./Albemarle Corporation for their
740 continued support of this and related research to improve the understanding of the hydrogeology
741 and geochemistry of the Salar de Atacama environment. The ASTER DEM and Landsat 8 OLI
742 were retrieved from EarthExplorer, courtesy of the NASA Land Processes Distributed Active
743 Archive Center, USGS/Earth Resources Observation and Science Center. Processed and
744 calibrated TRMM 2B31 dataset, a joint mission between NASA and the Japan Aerospace
745 Exploration Agency was kindly made publicly accessible by B. Bookhagen. The associate editor
746 and reviewer 2 are thanked for constructive comments that improved the manuscript.

747

748 **7. References**

- 749 Alley, W. M., R. W. Healy, J. W. LaBaugh, and T. E. Reilly (2002), Flow and storage in
750 groundwater systems., *Science*, 296(5575), 1985–1990, doi:10.1126/science.1067123.
- 751 Andermann, C., L. Longuevergne, S. Bonnet, A. Crave, P. Davy, and R. Gloaguen (2012),
752 Impact of transient groundwater storage on the discharge of Himalayan rivers, *Nat.*
753 *Geosci.*, 5(2), 127–132, doi:10.1038/ngeo1356.
- 754 Anderson, M., R. Low, and S. Foot (2002), Sustainable groundwater development in arid, high
755 Andean basins, *Geol. Soc. London, Spec. Publ.*, 193(1), 133–144,
756 doi:10.1144/GSL.SP.2002.193.01.11.
- 757 Aravena, R. (1995). Isotope Hydrology and Geochemistry of Northern Chile Groundwaters.
758 *Bull. IFEA*, 24, 495–503.
- 759 Aron, F., G. González, E. Veloso, and J. Cembrano (2008), Architecture and style of
760 compressive Neogene deformation in the eastern-southeastern border of the Salar de
761 Atacama Basin (22°30'-24°15'S): A structural setting for the active volcanic arc of the
762 Central Andes, *Int. Symp. Andean Geodyn.*, (1998), 52–55.
- 763 Barnes, C. J., & Allison, G. B. (1988). Tracing of water movement in the unsaturated zone using
764 stable isotopes of hydrogen and oxygen. *Journal of Hydrology*, 100(1–3), 143–176.
765 [https://doi.org/10.1016/0022-1694\(88\)90184-9](https://doi.org/10.1016/0022-1694(88)90184-9)
- 766 Bazuhair, A. S., and W. W. Wood (1996), Chloride mass-balance method for estimating ground
767 water recharge in arid areas: Examples from western Saudi Arabia, *J. Hydrol.*, 186(1-4),
768 153–159, doi:10.1016/S0022-1694(96)03028-4.
- 769 Betancourt, J. L., C. Latorre, J. A. Rech, J. Quade, and K. A. Rylander (2000), A 22,000-Year
770 Record of Monsoonal Precipitation from Northern Chile's Atacama Desert, *Science* (80-
771 .), 289(5484), 1542–1546, doi:10.1126/science.289.5484.1542.
- 772 Beria, H., Larsen, J. R., Ceperley, N. C., Michelon, A., Vennemann, T., & Schaepli, B. (2018).
773 Understanding snow hydrological processes through the lens of stable water isotopes.
774 *WIREs Water*, 5(6). <https://doi.org/10.1002/wat2.1311>
- 775 Blodgett, T. a., J. D. Lenters, and B. L. Isacks (1997), Constraints on the origin of paleolake
776 expansions in the Central Andes, *Earth Interact.*, 1(1), 1–1, doi:10.1175/1087-
777 3562(1997)001<0001:CotOoP>2.0.CO;2.
- 778 Bobst, A. L., T. K. Lowenstein, T. E. Jordan, L. V. Godfrey, T. L. Ku, and S. Luo (2001), A 106
779 ka paleoclimate record from drill core of the Salar de Atacama, northern Chile,
780 *Palaeogeogr. Palaeoclimatol. Palaeoecol.*, 173(1-2), 21–42, doi:10.1016/S0031-
781 0182(01)00308-X.
- 782 Bookhagen, B., and M. R. Strecker (2008), Orographic barriers, high-resolution TRMM rainfall,
783 and relief variations along the eastern Andes, *Geophys. Res. Lett.*, 35(6), 1–6,
784 doi:10.1029/2007GL032011.
- 785 Boutt D. F., Hynek S. A., Munk L. A., and Corenthal L. G. (2016) Rapid recharge of fresh water
786 to the halite-hosted brine aquifer of Salar de Atacama, Chile, *Hydrol. Process.*, 30: 4720–
787 4740. doi: 10.1002/hyp.10994.
- 788 Cervetto Sepulveda, M. M. (2012), Caracterización hidrogeológica e hidrogeoquímica de las
789 cuencas: Salar de Aguas Calientes 2, Puntas Negras, Laguna Tuyajto, Pampa Colorada,
790 Pampa las Tecas y Salar el Laco, II Region de Chile [M.S. Thesis], Universidad de Chile.

- 791 Condom, T., A. Coudrain, A. Dezetter, D. Brunstein, F. Delclaux, and S. Jean-Emmanuel (2004),
792 Transient modelling of lacustrine regressions: two case studies from the Andean
793 Altiplano, *Hydrol. Process.*, 18(13), 2395–2408, doi:10.1002/hyp.1470.
- 794 Condon, L. E., and R. M. Maxwell (2015), Evaluating the relationship between topography and
795 groundwater using outputs from a continental-scale integrated hydrology model, *Water*
796 *Resour. Res.*, 51, 6602–6621, doi:10.1002/2014WR016774.
- 797 Corenthal, L. G., D. F. Boutt, S. A. Hynek, and L. A. Munk (2016), Regional groundwater flow
798 and accumulation of a massive evaporite deposit at the margin of the Chilean Altiplano,
799 *Geophys. Res. Lett.*, 43, doi:10.1002/2016GL070076
- 800 Craig, H. (1961), Isotopic Variations in Meteoric Waters., *Science*, 133(3465), 1702–3,
801 doi:10.1126/science.133.3465.1702.
- 802 Crossey, L. J., T. P. Fischer, P. J. Patchett, K. E. Karlstrom, D. R. Hilton, D. L. Newell, P.
803 Huntoon, A. C. Reynolds, and G. a. M. de Leeuw (2006), Dissected hydrologic system at
804 the Grand Canyon: Interaction between deeply derived fluids and plateau aquifer waters
805 in modern springs and travertine, *Geology*, 34(1), 25, doi:10.1130/G22057.1.
- 806 Currell, M., Gleeson, T., & Dahlhaus, P. (2016). A new assessment framework for transience in
807 hydrogeological systems. *Groundwater*, 54(1), 4–14.
- 808 Cuthbert, M. O., Gleeson, T., Moosdorf, N., Befus, K. M., Schneider, A., Hartmann, J., &
809 Lehner, B. (2019, February 1). Global patterns and dynamics of climate–groundwater
810 interactions. *Nature Climate Change*. Nature Publishing Group.
811 <https://doi.org/10.1038/s41558-018-0386-4>
- 812 DePaolo, D. J., Conrad, M. E., Maher, K., & Gee, G. W. (2004). Evaporation Effects on Oxygen
813 and Hydrogen Isotopes in Deep Vadose Zone Pore Fluids at Hanford, Washington.
814 *Vadose Zone Journal*, 3(1), 220. <https://doi.org/10.2136/vzj2004.0220>
- 815 Dirección General de Aguas (2013), Análisis de la Oferta Hídrica del Salar de Atacama,
816 Santiago, Chile.
- 817 Dunai, T. J., G. a. González López, and J. Juez-Larré (2005), Oligocene-Miocene age of aridity
818 in the Atacama Desert revealed by exposure dating of erosion-sensitive landforms,
819 *Geology*, 33(4), 321–324, doi:10.1130/G21184.1.
- 820 Fritz, P., Suzuki, O., Silva, C., & Salati, E. (1981). Isotope hydrology of groundwaters in the
821 Pampa del Tamarugal, Chile. *Journal of Hydrology*, 53(1–2), 161–184.
822 [https://doi.org/10.1016/0022-1694\(81\)90043-3](https://doi.org/10.1016/0022-1694(81)90043-3)
- 823 Fritz, S. C., P. a. Baker, T. K. Lowenstein, G. O. Seltzer, C. a. Rigsby, G. S. Dwyer, P. M. Tapia,
824 K. K. Arnold, T. L. Ku, and S. Luo (2004), Hydrologic variation during the last 170,000
825 years in the southern hemisphere tropics of South America, *Quat. Res.*, 61(1), 95–104,
826 doi:10.1016/j.yqres.2003.08.007.
- 827 de la Fuente, A., Meruane, C., & Suárez, F. (2020). Long-term spatiotemporal variability in high
828 Andean wetlands in northern Chile. *Science of the Total Environment*.
829 <https://doi.org/10.1016/j.scitotenv.2020.143830>
- 830 Garreaud, R., M. Vuille, and A. C. Clement (2003), The climate of the Altiplano: Observed
831 current conditions and mechanisms of past changes, *Palaeogeogr. Palaeoclimatol.*
832 *Palaeoecol.*, 194(1-3), 5–22, doi:10.1016/S0031-0182(03)00269-4.
- 833 Gayo, E. M., C. Latorre, T. E. Jordan, P. L. Nester, S. A. Estay, K. F. Ojeda, and C. M. Santoro
834 (2012), Late Quaternary hydrological and ecological changes in the hyperarid core of the

- 835 northern Atacama Desert (~21°S), *Earth-Science Rev.*, 113(3-4), 120–140,
836 doi:10.1016/j.earscirev.2012.04.003.
- 837 Gelhar, L. W. & Wilson, J. L. Ground-Water Quality Modeling. *Ground Water* **12**, 399–408
838 (1974).
- 839 Gorelick, S. M., and C. Zheng (2015), Global change and the groundwater management
840 challenge, *Water Resour. Res.*, 51, 3031–3051, doi:10.1002/2014WR016825.
- 841 Gleeson, T., L. Marklund, L. Smith, and A. H. Manning (2011), Classifying the water table at
842 regional to continental scales, *Geophys. Res. Lett.*, 38(5), 1–6,
843 doi:10.1029/2010GL046427.
- 844 Gleeson, T., Y. Wada, M. F. P. Bierkens, and L. P. H. van Beek (2012), Water balance of global
845 aquifers revealed by groundwater footprint, *Nature*, 488(7410), 197–200,
846 doi:10.1038/nature11295.
- 847 Godfrey, L. V., T. E. Jordan, T. K. Lowenstein, and R. L. Alonso (2003), Stable isotope
848 constraints on the transport of water to the Andes between 22o and 26oS during the last
849 glacial cycle, *Palaeogeogr. Palaeoclimatol. Palaeoecol.*, 194(1-3), 299–317,
850 doi:10.1016/S0031-0182(03)00283-9.
- 851 Grosjean, M., M. A. Geyh, B. Messerli, and U. Schotterer (1995), Late-glacial and early
852 Holocene lake sediments, ground-water formation and climate in the Atacama Altiplano
853 22°24'S, *J. Paleolimnol.*, 14(3), 241–252, doi:10.1007/BF00682426.
- 854 Haitjema, H. M., and S. Mitchell-Bruker (2005), Are Water Tables a Subdued Replica of the
855 Topography?, *Ground Water*, 43(6), 781–786, doi:10.1111/j.1745-6584.2005.00090.x.
- 856 Hartley, A. J., and G. Chong (2002), Late Pliocene age for the Atacama Desert: Implications for
857 the desertification of western South America, *Geology*, 30(1), 43–46, doi:10.1130/0091-
858 7613(2002)030<0043:LPAFTA>2.0.CO;2.
- 859 Herrera Lameli, C. (2011), Informe Final Estudio Hidrogeologico Proyecto “ Planta de Sulfato
860 de Cobre Pentahidratado ,” , 0–33.
- 861 Herrera, C. et al., 2016. Groundwater flow in a closed basin with a saline shallow lake in a
862 volcanic area: Laguna Tuyajto, northern Chilean Altiplano of the Andes. *Science of the*
863 *Total Environment*, 541, p.303-318.
- 864 Herrera, C., Godfrey, L., Urrutia, J., Custodio, E., Jordan, T., Jódar, J., ... Barrenechea, F.
865 (2021). Recharge and residence times of groundwater in hyper arid areas: The confined
866 aquifer of Calama, Loa River Basin, Atacama Desert, Chile. *Science of the Total*
867 *Environment*, 752. <https://doi.org/10.1016/j.scitotenv.2020.141847>
- 868 Hoke, G. D., B. L. Isacks, T. E. Jordan, and J. S. Yu (2004), Groundwater-sapping origin for the
869 giant quebradas of northern Chile, *Geology*, 32(7), 605–608, doi:10.1130/G20601.1.
- 870 Houston, J. (2002). Groundwater recharge through an alluvial fan in the Atacama Desert,
871 northern Chile: Mechanisms, magnitudes and causes. *Hydrological Processes*, 16(15),
872 3019–3035. <https://doi.org/10.1002/hyp.1086>.
- 873 Houston, J. (2006a), Evaporation in the Atacama Desert: An empirical study of spatio-temporal
874 variations and their causes, *J. Hydrol.*, 330(3-4), 402–412,
875 doi:10.1016/j.jhydrol.2006.03.036.
- 876 Houston, J. (2006b), The great Atacama flood of 2001 and its implications for Andean
877 hydrology, *Hydrol. Process.*, 20(3), 591–610, doi:10.1002/hyp.5926.

- 878 Houston, J. (2007), Recharge to groundwater in the Turi Basin, northern Chile: An evaluation
879 based on tritium and chloride mass balance techniques, *J. Hydrol.*, 334(3-4), 534–544,
880 doi:10.1016/j.jhydrol.2006.10.030.
- 881 Houston, J. (2009), A recharge model for high altitude, arid, Andean aquifers, *Hydrol. Process.*,
882 23(16), 2383–2393, doi:10.1002/hyp.7350.
- 883 Houston, J., and D. Hart (2004), Theoretical head decay in closed basin aquifers: an insight into
884 fossil groundwater and recharge events in the Andes of northern Chile, *Quat. J. Eng.
885 Geol. Hydrogeol.*, 37(December 2007), 131–139, doi:10.1144/1470-9236/04-007.
- 886 Ibarra, D. E., & Chamberlain, C. P. (2015). Quantifying closed-basin lake temperature and
887 hydrology by inversion of oxygen isotope and trace element paleoclimate records.
888 *American Journal of Science*, 315(9), 781–808. <https://doi.org/10.2475/09.2015.01>
- 889 Ingebritsen SE, Manning CE (1999) Geological implications of a permeability-depth curve for
890 the continental crust. *Geology*, 27, 1,107–10.
- 891 Jayne, R. S., R. M. Pollyea, J. P. Dodd, E. J. Olson, and S. K. Swanson (2016), Spatial and
892 temporal constraints on regional-scale groundwater flow in the Pampa del Tamarugal
893 Basin, Atacama Desert, Chile, *Hydrogeol. J.*, (August), 1921–1937, doi:10.1007/s10040-
894 016-1454-3.
- 895 Johnson, E., J. Yáñez, C. Ortiz, and J. Muñoz (2010), Evaporation from shallow groundwater in
896 closed basins in the Chilean Altiplano, *Hydrol. Sci. J.*, 55(4), 624–635,
897 doi:10.1080/02626661003780458.
- 898 Jordan, T. E., N. Munoz, M. Hein, T. Lowenstein, L. Godfrey, and J. Yu (2002a), Active faulting
899 and folding without topographic expression in an evaporite basin, Chile, *Bull. Geol. Soc.
900 Am.*, 114(11), 1406–1421, doi:10.1130/0016-7606(2002)114<1406:AFAFWT>2.0.CO;2.
- 901 Jordan, T. E., L. V. Godfrey, N. Munoz, R. N. Alonso, T. K. Lowenstein, G. D. Hoke, N.
902 Peranginangin, B. L. Isacks, and L. Cathles (2002b), Orogenic-scale ground water
903 circulation in the Central Andes: evidence and consequences., 5th ISAG (International
904 Symp. Andean Geodyn., 331–334.
- 905 Jordan, T. E., C. Mpodozis, N. Muñoz, N. Blanco, P. Pananont, and M. Gardeweg (2007),
906 Cenozoic subsurface stratigraphy and structure of the Salar de Atacama Basin, northern
907 Chile, *J. South Am. Earth Sci.*, 23(2-3), 122–146, doi:10.1016/j.jsames.2006.09.024.
- 908 Jordan, T., C. Herrera Lameli, N. Kirk-Lawlor, and L. Godfrey (2015), Architecture of the
909 aquifers of the Calama Basin, Loa catchment basin, northern Chile, *Geosphere*, 11(5),
910 GES01176.1, doi:10.1130/GES01176.1.
- 911 Jordan, T. E., Herrera L., C., Godfrey, L. V., Colucci, S. J., Gamboa P., C., Urrutia M., J., ...
912 Paul, J. F. (2019). Isotopic characteristics and paleoclimate implications of the extreme
913 precipitation event of march 2015 in Northern Chile. *Andean Geology*, 46(1), 1–31.
914 <https://doi.org/10.5027/andgeov46n1-3087>
- 915 Kampf, S. K., and S. W. Tyler (2006), Spatial characterization of land surface energy fluxes and
916 uncertainty estimation at the Salar de Atacama, Northern Chile, *Adv. Water Resour.*,
917 29(2), 336–354, doi:10.1016/j.advwatres.2005.02.017.
- 918 Kikuchi, C. P., & Ferré, T. P. A. (2017). Analysis of subsurface temperature data to quantify
919 groundwater recharge rates in a closed Altiplano basin, northern Chile. *Hydrogeology
920 Journal*, 25(1), 103–121. <https://doi.org/10.1007/s10040-016-1472-1>.
- 921 Lamb, S., and P. Davis (2003), Cenozoic climate change as a possible cause for the rise of the
922 Andes., *Nature*, 425(6960), 792–797, doi:10.1038/nature02049.

- 923 Lasaga, A. C. & Berner, R. A. Fundamental aspects of quantitative models for geochemical
924 cycles. *Chem. Geol.* 145, 161–175 (1998).
- 925 Liu, Y., Wagener, T., Beck, H. E., & Hartmann, A. (2020). What is the hydrologically effective
926 area of a catchment? *Environmental Research Letters*, 15(10).
927 <https://doi.org/10.1088/1748-9326/aba7e5>
- 928 Lowenstein, T. K., and F. Risacher (2009), Closed basin brine evolution and the influence of Ca–
929 Cl inflow waters: Death Valley and Bristol Dry Lake California, Qaidam Basin, China,
930 and Salar de Atacama, Chile, *Aquat. Geochem.*, 15, 71–94, doi:10.1007/s10498-008-
931 9046-z.
- 932 Lowenstein, T. K., M. C. Hein, A. L. Bobst, T. E. Jordan, T.-L. Ku, and S. Luo (2003), An
933 Assessment of stratigraphic completeness in climate-sensitive closed-basin lake
934 sediments: Salar de Atacama, Chile, *J. Sediment. Res.*, 73(1), 91–104,
935 doi:10.1306/061002730091.
- 936 Magaritz, M., Aravena, R., Peña, H., Suzuki, O., & Grilli, A. (1989). Water chemistry and
937 isotope study of streams and springs in northern Chile. *Journal of Hydrology*, 108(C),
938 323–341. [https://doi.org/10.1016/0022-1694\(89\)90292-8](https://doi.org/10.1016/0022-1694(89)90292-8)
- 939 Magaritz, M., R. Aravena, H. Pena, O. Suzuki, and A. Grilli (1990), Source of ground water in
940 the deserts of Northern Chile: Evidence of deep circulation of ground water from the
941 Andes, *Ground Water*, 28(4), 513–517, doi:10.1111/j.1745-6584.1990.tb01706.x.
- 942 Marazuela, M. A., Vázquez-Suñé, E., Custodio, E., Palma, T., García-Gil, A., & Ayora, C.
943 (2018). 3D mapping, hydrodynamics and modelling of the freshwater-brine mixing zone
944 in salt flats similar to the Salar de Atacama (Chile). *Journal of Hydrology*, 561, 223–235.
945 <https://doi.org/10.1016/j.jhydrol.2018.04.010>
- 946 Marazuela, M. A., Vázquez-Suñé, E., Ayora, C., García-Gil, A., & Palma, T. (2019).
947 Hydrodynamics of salt flat basins: The Salar de Atacama example. *Science of the Total*
948 *Environment*, 651, 668–683. <https://doi.org/10.1016/j.scitotenv.2018.09.190>
- 949 Marazuela, M. A., Vázquez-Suñé, E., Ayora, C., & García-Gil, A. (2020a). Towards more
950 sustainable brine extraction in salt flats: Learning from the Salar de Atacama. *Science of*
951 *the Total Environment*, 703. <https://doi.org/10.1016/j.scitotenv.2019.135605>
- 952 Marazuela, M. A., Ayora, C., Vázquez-Suñé, E., Olivella, S., & García-Gil, A. (2020b).
953 Hydrogeological constraints for the genesis of the extreme lithium enrichment in the
954 Salar de Atacama (NE Chile): A thermohaline flow modelling approach. *Science of the*
955 *Total Environment*, 739. <https://doi.org/10.1016/j.scitotenv.2020.139959>
- 956 Mardones, L. (1986), Características geológicas e hidrogeológicas del Salar de Atacama, in *El*
957 *litio: Un nuevo recurso para Chile*, edited by G. Lagos, pp. 181–216, Universidad de
958 Chile, Santiago, Chile.
- 959 Martínez, F., López, C., Bascuñan, S., & Arriagada, C. (2018). Tectonic interaction between
960 Mesozoic to Cenozoic extensional and contractional structures in the Preandean
961 Depression (23°–25°S): Geologic implications for the Central Andes. *Tectonophysics*,
962 744, 333–349. <https://doi.org/10.1016/j.tecto.2018.07.016>
- 963 Masbruch, M. D., C. A. Rumsey, S. Gangopadhyay, D. D. Susong, and T. Pruitt (2016),
964 Analyses of infrequent (quasi-decadal) large groundwater recharge events in the northern
965 Great Basin: Their importance for groundwater availability, use, and management, *Water*
966 *Resour. Res.*, 52, doi:10.1002/2016WR019060.

- 967 Maxwell, P. (2014), Analysing the lithium industry: Demand, supply, and emerging
968 developments, *Miner. Econ.*, 26(3), 97–106, doi:10.1007/s13563-013-0041-5.
- 969 Meijer, A. & Kwicklis, E. (2000). Geochemical and isotopic constraints on ground-water flow
970 directions, mixing and recharge at Yucca Mountain, Nevada, United States.
971 <https://doi.org/10.2172/883407>
- 972 McDonald, M. G., and A. W. Harbaugh (1988), A modular three-dimensional finite-difference
973 ground-water flow model, United States Geological Survey.
- 974 McGuire, K. J., and J. J. McDonnell (2010), Hydrological connectivity of hillslopes and streams:
975 Characteristic time scales and nonlinearities, *Water Resour. Res.*, 46, W10543,
976 doi:10.1029/2010WR009341.
- 977 McNamara, J. P., D. Tetzlaff, K. Bishop, C. Soulsby, M. Seyfried, N. E. Peters, B. T. Aulenbach,
978 and R. Hooper (2011), Storage as a metric of catchment comparison, *Hydrol. Processes*,
979 25, 3364–3371.
- 980 Montgomery, E. L., M. J. Rosko, S. O. Castro, B. R. Keller, and P. S. Bevacqua (2003),
981 Interbasin underflow between closed Altiplano basins in Chile., *Ground Water*, 41(4),
982 523–31.
- 983 Moran, B. J., Boutt, D. F., & Munk, L. A. (2019). Stable and Radioisotope Systematics Reveal
984 Fossil Water as Fundamental Characteristic of Arid Orogenic-Scale Groundwater
985 Systems. *Water Resources Research*, 55. <https://doi.org/10.1029/2019WR026386>
- 986 Munk, L.A., Hynek, S.A., Bradley, D.C., Boutt, D.F., Labay, K., Jochens, H., 2016. Lithium
987 Brines: A Global Perspective, in Verplanck, P.L. and Hitzman, M.W., eds., *Rare Earth and*
988 *Critical Elements in Ore Deposits. Reviews in Economic Geology* (18), 339–365.
- 989 Munk, L. A., Boutt, D. F., Hynek, S. A., & Moran, B. J. (2018). Hydrogeochemical fluxes and
990 processes contributing to the formation of lithium-enriched brines in a hyper-arid
991 continental basin. *Chemical Geology*, 493, 37–57.
992 <https://doi.org/10.1016/j.chemgeo.2018.05.013>
- 993 Muñoz, Enrique, Álvarez, César, Billib, Max, Arumí, José Luis, & Rivera, Diego. (2011).
994 Comparison of Gridded and Measured Rainfall Data for Basin-scale Hydrological
995 Studies. *Chilean Journal of agricultural research*, 71(3), 459-468. doi: 10.4067/S0718-
996 58392011000300018
- 997 Muñoz, E., Arumí, J. L., Wagener, T., Oyarzún, R., & Parra, V. (2016). Unraveling complex
998 hydrogeological processes in Andean basins in south-central Chile: An integrated
999 assessment to understand hydrological dissimilarity. *Hydrological Processes*, 30(26),
1000 4934–4943. <https://doi.org/10.1002/hyp.11032>
- 1001 Nelson, S.T., Anderson, K.W., and Mayo, A.L., 2004, Testing the interbasin flow hypothesis at
1002 Death Valley, CA, USA: *Eos*, v. 85, p. 349, 355-356.
- 1003 Nelson, S.T., and Mayo, A.L., 2014, The role of interbasin groundwater transfers in geologically
1004 complex terranes, demonstrated by the Great Basin in the western United States:
1005 *Hydrogeology Journal*, v. 22, p. 807-822, DOI 10.1007/s10040-014-1104-6.
- 1006 Pérez-Fodich, A., M. Reich, F. Álvarez, G. T. Snyder, R. Schoenberg, G. Vargas, Y. Muramatsu,
1007 and U. Fehn (2014), Climate change and tectonic uplift triggered the formation of the
1008 atacama desert's giant nitrate deposits, *Geology*, 42(3), 251–254, doi:10.1130/G34969.1.
- 1009 Placzek, C., J. Quade, and P. J. Patchett (2006), Geochronology and stratigraphy of late
1010 Pleistocene lake cycles on the southern Bolivian Altiplano: Implications for causes of
1011 tropical climate change, *Bull. Geol. Soc. Am.*, 118(5-6), 515–532, doi:10.1130/B25770.1.

- 1012 Placzek, C. J., J. Quade, and P. J. Patchett (2013), A 130ka reconstruction of rainfall on the
1013 Bolivian Altiplano, *Earth Planet. Sci. Lett.*, 363, 97–108, doi:10.1016/j.epsl.2012.12.017.
- 1014 Quade, J., J. a. Rech, J. L. Betancourt, C. Latorre, B. Quade, K. A. Rylander, and T. Fisher
1015 (2008), Paleowetlands and regional climate change in the central Atacama Desert,
1016 northern Chile, *Quat. Res.*, 69(3), 343–360, doi:10.1016/j.yqres.2008.01.003.
- 1017 Ramirez, C., and M. Gardeweg (1982), *Carta Geologica de Chile, escala 1:250000, Hoja*
1018 *Toconao, Region de Antofagasta, Chile No. 54, Santiago, Chile.*
- 1019 Rech, J. a, J. L. Betancourt, and J. Quade (2002), Late Quaternary paleohydrology of the central
1020 Atacama Desert (lat 22 -24 S), Chile, *Geol. Soc. Am. Bull.*, 114(3), 334–348,
1021 doi:10.1130/0016-7606(2002)114<0334:LQPOTC>2.0.CO;2.
- 1022 Rech, J. a., J. S. Pigati, J. Quade, and J. L. Betancourt (2003), Re-evaluation of mid-Holocene
1023 deposits at Quebrada Puripica, northern Chile, *Palaeogeogr. Palaeoclimatol. Palaeoecol.*,
1024 194, 207–222, doi:10.1016/S0031-0182(03)00278-5.
- 1025 Reutter, K.-J. et al. (2006), The Salar de Atacama Basin : A Subsiding block within the western
1026 edge of the Altiplano-Puna Plateau, *Andes. Act. Subduction Orogeny*, 303–325.
- 1027 Risacher, F., H. Alonso, and C. Salazar (2003), The origin of brines and salts in Chilean salars: A
1028 hydrochemical review, *Earth-Science Rev.*, 63(3-4), 249–293, doi:10.1016/S0012-
1029 8252(03)00037-0.
- 1030 Rissmann, C., M. Leybourne, C. Benn, and B. Christenson (2015), The origin of solutes within
1031 the groundwaters of a high Andean aquifer, *Chem. Geol.*, 396, 164–181,
1032 doi:10.1016/j.chemgeo.2014.11.029.
- 1033 Rubilar, J., Martínez, F., Arriagada, C., Becerra, J., 2017. Structure of the Cordillera de la Sal: A
1034 key tectonic element for the Oligocene-Neogene evolution of the Salar de Atacama basin,
1035 Central Andes, northern Chile. *J. S. Am. Earth Sci.*
1036 <https://doi.org/10.1016/j.jsames.2017.11.013>.
- 1037 Sáez, A., Godfrey, L.V., Herrera, C., Chong, G., and Pueyo, J. J. (2016), Timing of wet episodes
1038 in Atacama Desert over the last 15 ka. *The Groundwater Discharge Deposits (GWD)*
1039 *from Domeyko Range at 25°S.*, *Quaternary Science Reviews*, Vol. 145, 82-93,
1040 doi:10.1016/j.quascirev.2016.05.036.
- 1041 Salas, J., J. Guimerà, O. Cornellà, R. Aravena, E. Guzmán, C. Tore, W. Von Igel, and R. Moreno
1042 (2010), Hidrogeología del sistema lagunar del margen este del Salar de Atacama (Chile),
1043 *Bol. Geol. y Min.*, 121(4), 357–372.
- 1044 Salisbury, M. J., B. R. Jicha, S. L. de Silva, B. S. Singer, N. C. Jiménez, and M. H. Ort (2011),
1045 ⁴⁰Ar/³⁹Ar chronostratigraphy of Altiplano-Puna volcanic complex ignimbrites reveals
1046 the development of a major magmatic province, *Bull. Geol. Soc. Am.*, 123(5), 821–840,
1047 doi:10.1130/B30280.1.
- 1048 Santoro, C.M., Gayo, E.M., Capriles, J.M., de Porras, M.E., Maldonado, A., Standen, V.G.,
1049 Latorre, C., Castro, V., Angelo, D., McRostie, V., Uribe, M., Valenzuela, D., Ugalde,
1050 P.C., Marquet, P.A. (2017). Continuities and discontinuities in the socio-environmental
1051 systems of the Atacama Desert during the last 13,000 years. *Journal of Anthropological*
1052 *Archaeology* 46, 28–39
- 1053 Scanlon, B. R., K. E. Keese, A. L. Flint, L. E. Flint, C. B. Gaye, W. M. Edmunds, and I.
1054 Simmers (2006), Global synthesis of groundwater recharge in semiarid and arid regions,
1055 *Hydrol. Process.*, 20(15), 3335–3370, doi:10.1002/hyp.6335.

- 1056 Scheihing, K. W., Moya, C. E., Struck, U., Lictevout, E., & Tröger, U. (2018). Reassessing
1057 hydrological processes that control stable Isotope Tracers in groundwater of the Atacama
1058 Desert (Northern Chile). *Hydrology*, 5(1). <https://doi.org/10.3390/hydrology5010003>.
- 1059 Schaller, M. F., and Y. Fan (2009), River basins as groundwater exporters and importers:
1060 Implications for water cycle and climate modeling, *J. Geophys. Res. Atmos.*, 114(4),
1061 doi:10.1029/2008JD010636.
- 1062 Sociedad Chilena de Litio Ltda. (2009), Informe Hidrología e Hidrogeología Adenda 1 - EIA
1063 Modificaciones y Mejoramiento del Sistema de Pozas de Evaporación Solar en el Salar
1064 de Atacama, Antofagasta, Chile.
- 1065 Sprenger, M., Herbstritt, B., & Weiler, M. (2015). Established methods and new opportunities
1066 for pore water stable isotope analysis. *Hydrological Processes*, 29(25), 5174–5192.
1067 <https://doi.org/10.1002/hyp.10643>.
- 1068 Stigter, E. E., Litt, M., Steiner, J. F., Bonekamp, P. N. J., Shea, J. M., Bierkens, M. F. P., &
1069 Immerzeel, W. W. (2018). The Importance of Snow Sublimation on a Himalayan Glacier.
1070 *Frontiers in Earth Science*, 6. <https://doi.org/10.3389/feart.2018.00108>
- 1071 Tóth, J. (1963), A theoretical analysis of groundwater flow in small drainage basins, *J. Geophys.*
1072 *Res.*, 68(16), 4795–4812, doi:10.1029/JZ068i016p04795.
- 1073 Tyler, S. W., J. F. Muñoz, and W. W. Wood (2006), The response of playa and sabkha
1074 hydraulics and mineralogy to climate forcing, *Ground Water*, 44(3), 329–338,
1075 doi:10.1111/j.1745-6584.2005.00096.x.
- 1076 Urbano, I. D., M. Person, K. Kelts, and J. S. Hanor (2004), Transient groundwater impacts on the
1077 development of paleoclimatic lake records in semi-arid environments, *Geofluids*, 4(3),
1078 187–196, doi:10.1111/j.1468-8123.2004.00081.x.
- 1079 Uribe, J., Muñoz, J.F., Gironás, J. Oyarzún, R., Aguirre, E. and Aravena, R. (2016) Assessing
1080 groundwater recharge in an Andean closed basin using isotopic characterization and a
1081 rainfall-runoff model: Salar del Huasco basin, Chile, *Hydrogeology Journal* 23 (7), 1535-
1082 1551.
- 1083 Urrutia, J., Herrera, C., Custodio, E., Jódar, J., & Medina, A. (2019). Groundwater recharge and
1084 hydrodynamics of complex volcanic aquifers with a shallow saline lake: Laguna Tuyajto,
1085 Andean Cordillera of northern Chile. *Science of the Total Environment*, 697.
1086 <https://doi.org/10.1016/j.scitotenv.2019.134116>.
- 1087 van Beek, L. P. H., Y. Wada, and M. F. P. Bierkens (2011), Global monthly water stress: 1.
1088 Water balance and water availability, *Water Resour. Res.*, 47, W07517,
1089 doi:10.1029/2010WR009791
- 1090 Viguier, B., Jourde, H., Yáñez, G., Lira, E. S., Leonardi, V., Moya, C. E., ... Lictevout, E.
1091 (2018). Multidisciplinary study for the assessment of the geometry, boundaries and
1092 preferential recharge zones of an overexploited aquifer in the Atacama Desert (Pampa del
1093 Tamarugal, Northern Chile). *Journal of South American Earth Sciences*, 86, 366–383.
1094 <https://doi.org/10.1016/j.jsames.2018.05.018>.
- 1095 Viguier, B., Jourde, H., Leonardi, V., Lictevout, E., & Daniele, L. (2020). Water table variations
1096 in atacama desert alluvial fans: Discussion of “evidence of short-term groundwater
1097 recharge signal propagation from the andes to the central atacama desert: A singular
1098 spectrum analysis approach.” *Hydrological Sciences Journal*, 65(9), 1606–1613.
1099 <https://doi.org/10.1080/02626667.2020.1764001>.

- 1100 Vuille, M., and C. Ammann (1997), Regional snowfall patterns in the high, arid Andes, *Clim.*
1101 *Change*, 36, 413–423, doi:10.1007/978-94-015-8905-5_10.
- 1102 Ward, K. M., G. Zandt, S. L. Beck, D. H. Christensen, and H. McFarlin (2014), Seismic imaging
1103 of the magmatic underpinnings beneath the Altiplano-Puna volcanic complex from the
1104 joint inversion of surface wave dispersion and receiver functions, *Earth Planet. Sci. Lett.*,
1105 404, 43–53, doi:10.1016/j.epsl.2014.07.022.
- 1106

1107 FIGURE CAPTIONS:

1108 **Figure 1:** Location map and cross-section of elevation and precipitation for the Salar de Atacama
1109 region of 21 to 25° S. (a) Elevations (0 to > 6,000 m) from an Advanced Spaceborne Thermal
1110 Emission and Reflection Radiometer (ASTER) Global Digital Elevation Model (GDEM). Gages
1111 maintained by the Chilean DGA. (b) Simplified geologic map of the A-A' cross section showing
1112 approximate location of chloride mass balance (CMB) sampling sites (modified from Moran et
1113 al., 2019). (c) ASTER GDEM derived elevation and TRMM 2B31 estimates of MAP from 1998
1114 to 2009.

1115 **Figure 2:** (a) Stable isotopic composition of water samples considered for CMB calculations.
1116 Samples collected as part of this study and from *Cervetto* [2012]. Only samples of inflow
1117 groundwater close to the global meteoric water line, shown as solid black diamonds, were
1118 selected for the CMB calculations. (b) Stable isotopic composition of groundwater samples
1119 within the topographic watershed used for CMB analysis. CMB cutoff is deuterium excess <5
1120 ‰.

1121 **Figure 3** Results of chloride mass balance (CMB). (a) GWR determined by the CMB method
1122 based on samples in the Salar de Atacama, Linzor basin, and Chilean Puna Plateau. Uncertainty
1123 includes a range of Cl in precipitation from 5–16 mg/L. MAP from the TRMM 2B31 dataset.
1124 Solid line is the best fit to calculated CMB results, while the dashed line shows the infiltration
1125 rate required to close the steady state hydrologic budget in the Salar de Atacama topographic
1126 watershed. (b) Frequency distribution of gridded (25 km²) MAP from the TRMM 2B31 dataset
1127 within the topographic watershed.

1128 **Figure 4** Spatial distribution of precipitation (P), groundwater recharge (GWR) for the median
1129 precipitation scenario, and potential evapotranspiration (PET) used to evaluate the topographic
1130 and regional scale hydrologic budget of the Salar de Atacama. (a) mean annual precipitation
1131 from 1998–2009 based on the TRMM 2B31 dataset. Black circles are groundwater Cl sample
1132 locations. (b) Median annual GWR from 1998-2009 determined by applying equation (2) to
1133 median precipitation dataset. (c) PET determined as a function of elevation applied to discharge
1134 zones (gray polygons), excluding Salar de Atacama.

1135 **Figure 5** a) Regional watersheds from Corenthal et al. (2016) for the evaluation, the steady state
1136 contributing regions for the Salar de Atacama, and Rio Loa Basins using full uncertainty
1137 considerations for the water balance. Each lettered zone for Salar de Atacama includes the
1138 cumulative area of all smaller zones. A is the topographic watershed, and M is the inferred
1139 hydrogeologic watershed where $GWR+R$ balances ET in the full uncertainty bounds. The Rio
1140 Loa contributing areas are from Jordan et al. (2015). Background is an ASTER DEM. Dashed
1141 line indicates the position of the 2-D model presented in Figure 6. Numbered locations refer to
1142 modern and paleo hydraulic head estimates in Figures 7 and 8. b) Chloride mass balance
1143 recharge + runoff estimates (blue diamonds) for lower (light blue) and upper bound recharge
1144 (dark blue) scenarios. Evapotranspiration bounds (red diamonds) for lower (light red) and upper
1145 estimates (dark red). Letters indicate the areas represented by the black polygons in a).

1146 **Figure 6** Model geometry, boundary conditions, hydraulic conductivity distribution, and initial
1147 water table positions for the restrictive and conducive simulations described in text.

1148 **Figure 7** Simulated hydraulic head distributions for (a) restrictive and (b) conducive simulations
1149 at time of 0, 1000, 10000, 100000 years after change in recharge. Position of the hydrogeologic
1150 divides is shown for labeled times in vertical black lines. Numbered locations correspond to
1151 head observation locations plotted in Figure 8.

1152 **Figure 8** Simulated hydraulic heads (y-axis) for restrictive and conducive simulations compared
1153 to modern field and paleo-hydraulic head estimates (x-axis). Sizes of colored polygons (pink –
1154 conducive, blue – restrictive) are based on simulated heads with the highest position being the
1155 initial condition for the models. Highest observed heads are estimated based on paleo-hydrologic
1156 information cited in the text and presented in the Supporting Information 5.

1157 **Figure 9** Plot of the ratio of discharge from constant head cells at Salar de Atacama and drains
1158 along the plateau margin (D_{SdA}) to specified total model recharge ($GW_{TOTALRCH}$). The unshaded
1159 region represents discharge to Salar de Atacama that is greater than total model recharge (i.e.
1160 some contribution of groundwater storage). The shaded areas represent times in the simulation
1161 where discharge to Salar de Atacama is less than the total model recharge.

1162

1163 **Figure 10** Compilation of recharge rates summarized from the literature (including this study)
1164 with a focus on the arid regions of northern Chile. Estimates are from a range of methods
1165 including water/energy balance, heat tracing, and chloride mass balance and are differentiated
1166 based on whether they are point measurements or basin scale recharge rates.

1167

1168

1169

1170 TABLE CAPTIONS:

1171 **Table 1:** Locations and characteristics of precipitation samples used to determine chloride
1172 concentrations in precipitation

1173 **Table 2:** Predicted precipitation and recharge for topographic and hydrogeologic catchments

1174 **Table 3:** Tabulated attributes and results of groundwater chloride analyses including estimates of
1175 groundwater recharge from the CMB method.

1176

1177

1178

1179

1180

1181

1182

1183

1184

1185

1186

1187

1188

1189

1190

1191

1192

1193

1194

1195

1196

1197

1198

1199
1200
1201
1202
1203
1204
1205
1206
1207
1208
1209
1210
1211
1212
1213
1214
1215
1216
1217
1218
1219

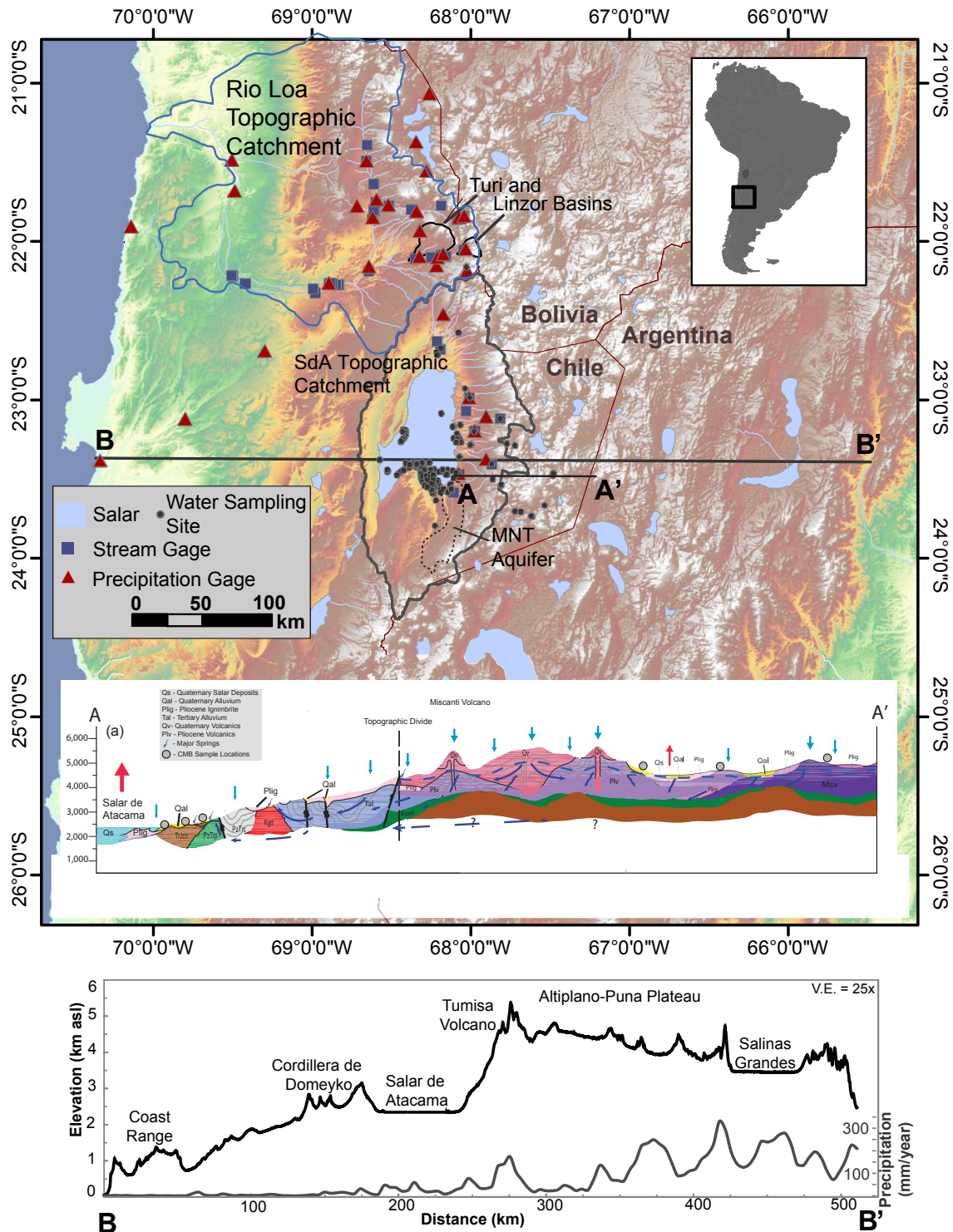


Figure 1: Location map and cross-section of elevation and precipitation for the SdA region of 21 to 25° S. (a) Elevations (0 to > 6,000 m) from an Advanced Spaceborne Thermal Emission and Reflection Radiometer (ASTER) Global Digital Elevation Model (GDEM). Gages maintained by the Chilean DGA. (b) Simplified geologic map across the line A-A' on (a) modified from Moran et al., 2009 (c) ASTER GDEM derived elevation and TRMM 2B31 estimates of MAP from 1998 to 2009.

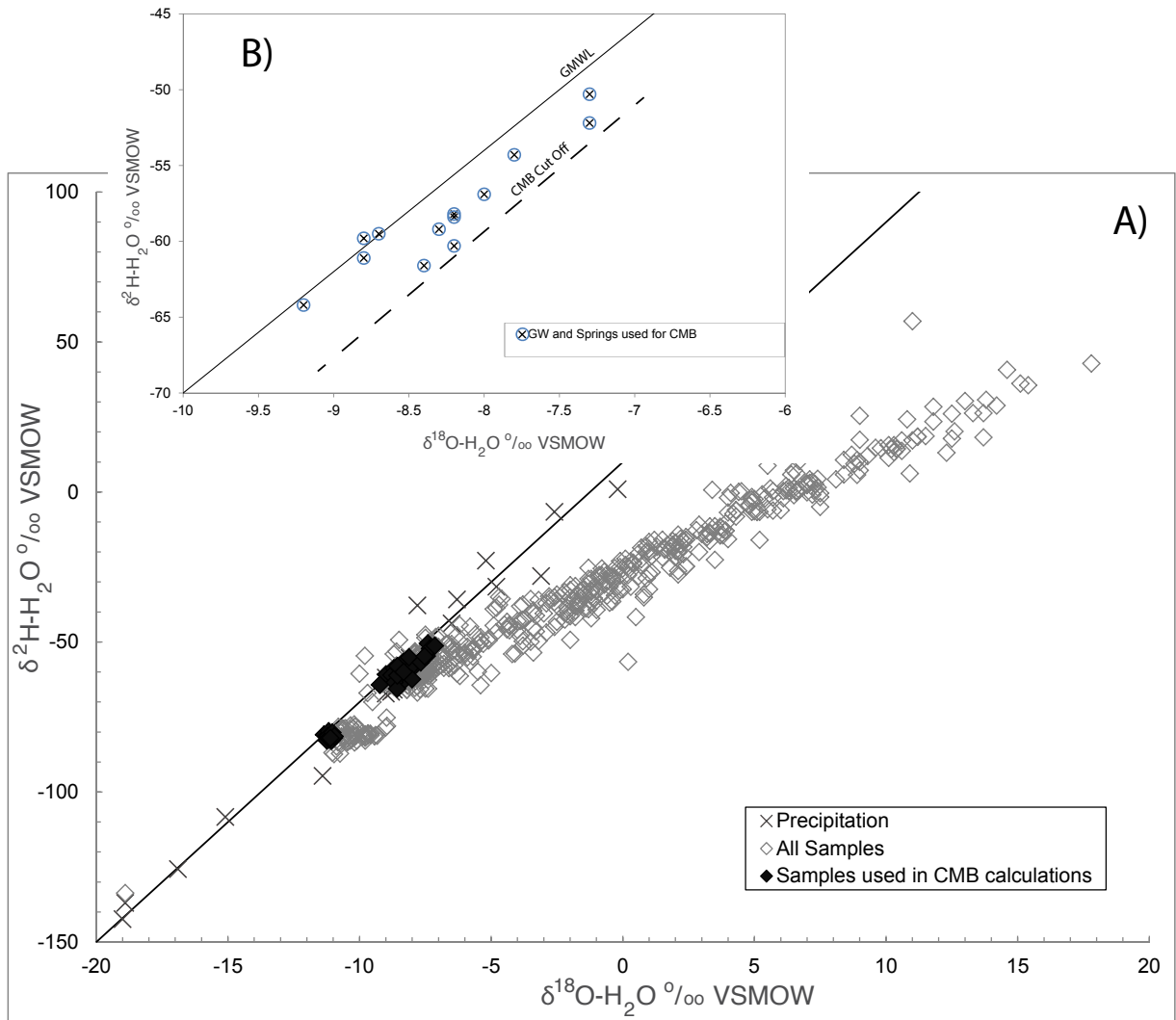


Figure 2: (a) Stable isotopic composition of samples considered for CMB calculations. Samples collected as part of this study and from Cervetto [2012]. Only samples of inflow groundwater that plot closely to the global meteoric water line, shown as solid black diamonds, were selected for the CMB calculations. (b) Stable isotopic composition of groundwater samples within the topographic watershed used for CMB analysis. CMB cutoff is deuterium excess $<5\text{‰}$.

1221
 1222
 1223
 1224
 1225
 1226
 1227
 1228

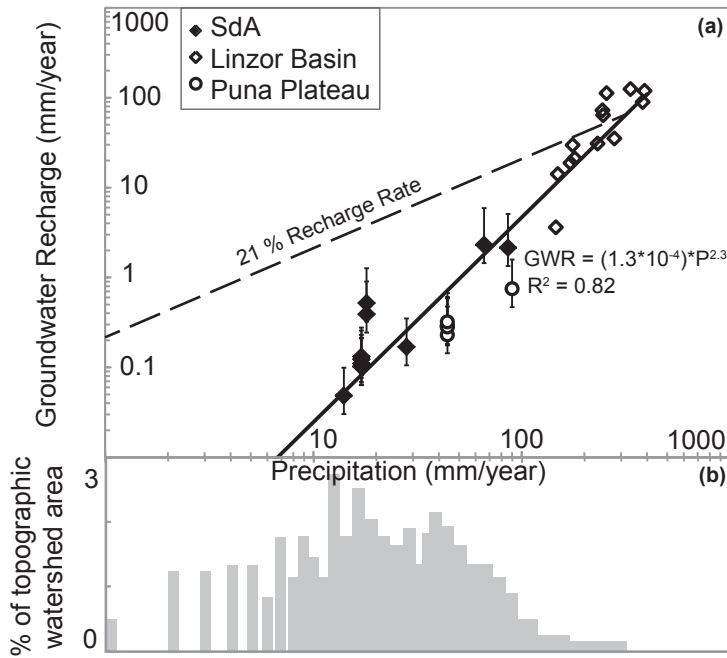


Figure 3 Results of chloride mass balance (CMB). (a) GWR determined by the CMB method based on samples in the SdA, Linzor basin and Chilean Puna Plateau. Uncertainty includes a range of Cl in precipitation from 5–16 mg/l. MAP from the TRMM 2B31 dataset. Solid line is the best fit to calculated CMB results, while the dashed line shows the infiltration rate required to close the steady state hydrologic

1229
 1230
 1231
 1232
 1233
 1234
 1235
 1236
 1237
 1238
 1239
 1240
 1241

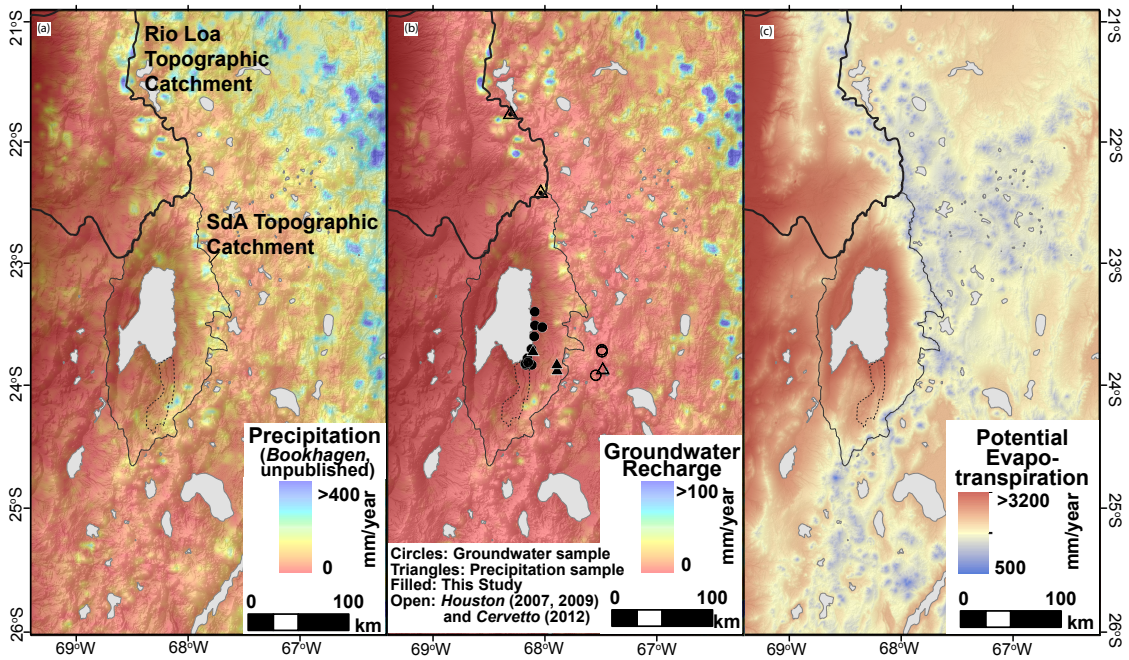


Figure 4 Spatial distribution of P, GWR for the median precipitation scenario and PET used to evaluate the topographic and regional scale hydrologic budget of the SdA. (a) MAP from 1998–2009 based on TRMM 2B31 dataset. Black circles are groundwater CI sample locations. (b) Median annual GWR from 1998–2009 determined by applying equation (2) to median precipitation dataset. (c) PET determined as a function of elevation applied to discharge zones (gray polygons), excluding SdA.

1242
1243
1244
1245
1246
1247
1248
1249

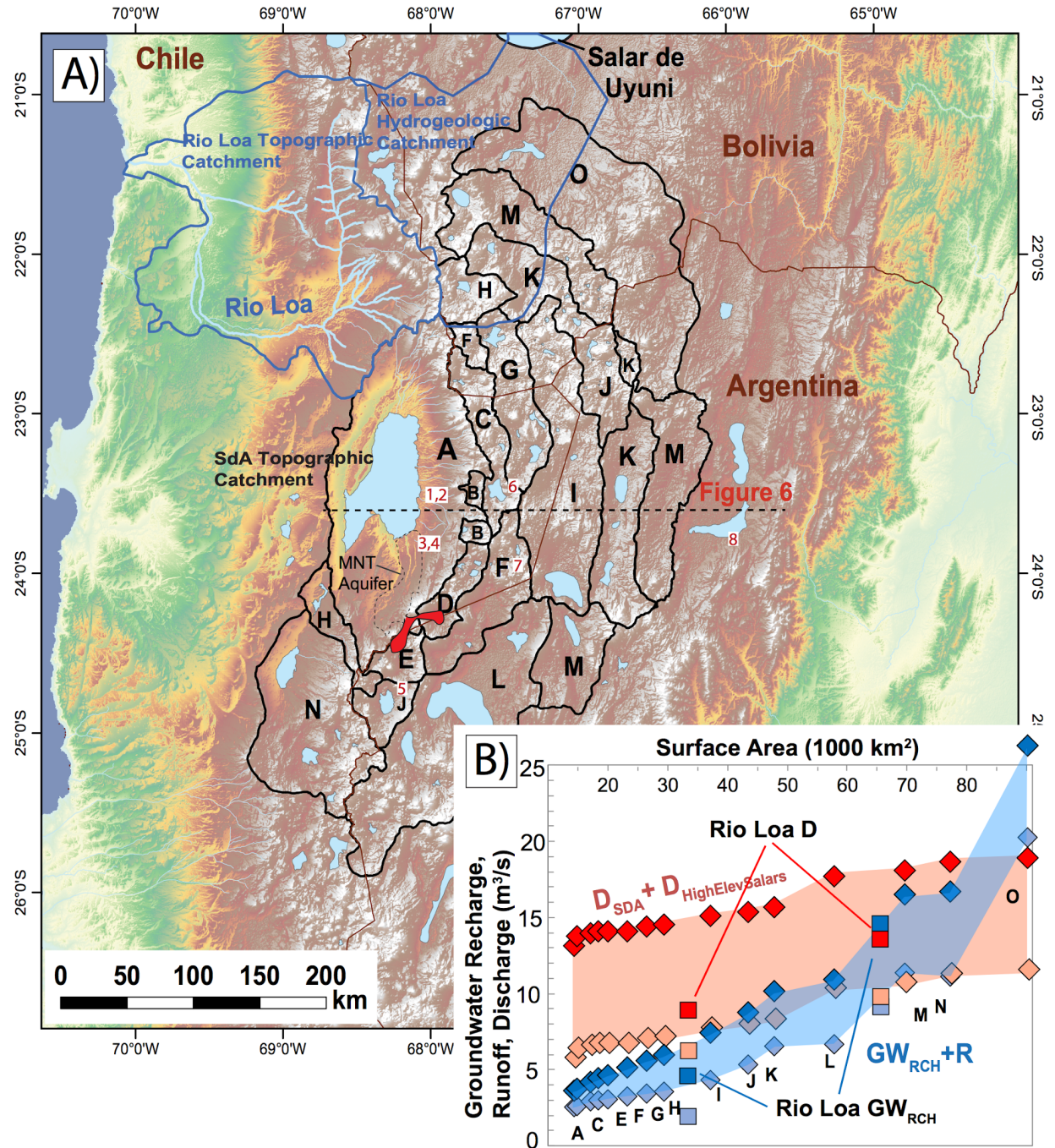


Figure 5 A) Regional watersheds from Corenthal et al. (2016) for the evaluation the steady state contributing regions for the Salar de Atacama and Rio Loa Basins using full uncertainty considerations for the water balance. Each lettered zone for SdA includes the cumulative area of all smaller zones. A is the topographic watershed, and M is the inferred hydrogeologic watershed where GWR+R balances ET in the full uncertainty bounds. The Rio Loa contributing areas are from Jordan et al. (2015). Background is an ASTER DEM. Dashed line indicates the position of the 2-D model presented in Figure 6. Numbered locations refer to modern and paleo hydraulic head estimates in Figures 7 and 8. B) Chloride mass balance recharge + runoff estimates (blue diamonds) for lower (light blue) and upper bound recharge (dark blue) scenarios. Evapotranspiration bounds (red diamonds) for lower (light red) and upper estimates (dark red). Letters indicate the areas represented by the black polygons in A).

1250
1251
1252

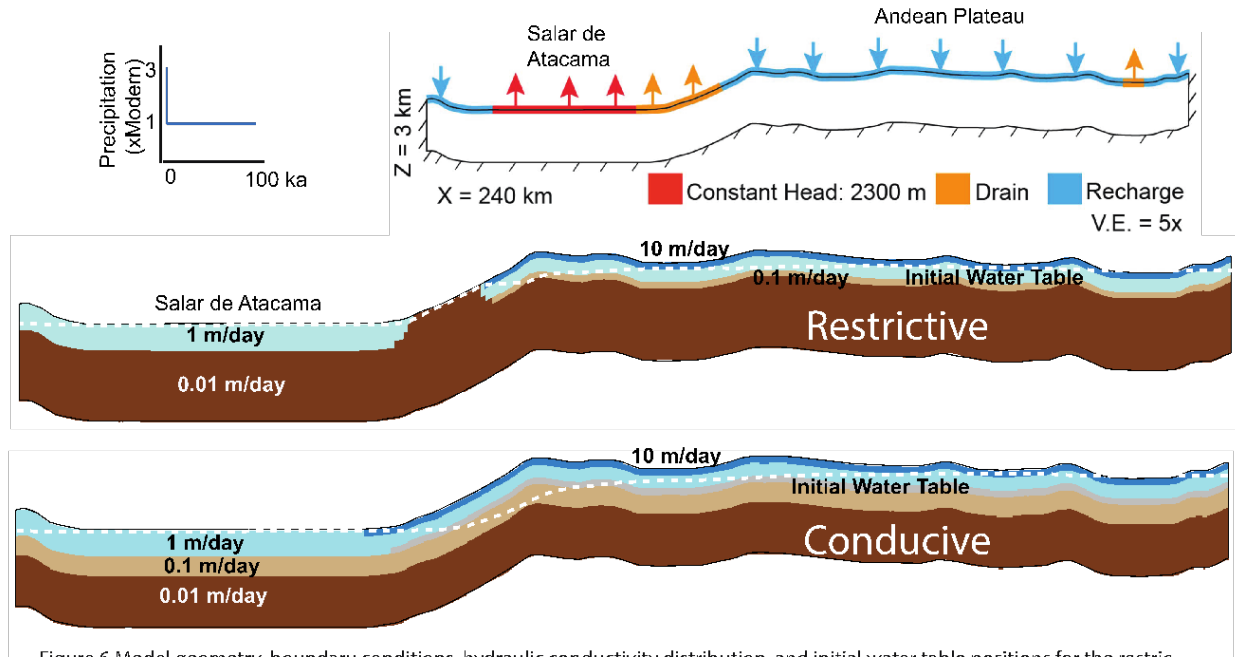


Figure 6 Model geometry, boundary conditions, hydraulic conductivity distribution, and initial water table positions for the restrictive and conductive simulations described in text.

1253
1254
1255
1256
1257
1258
1259

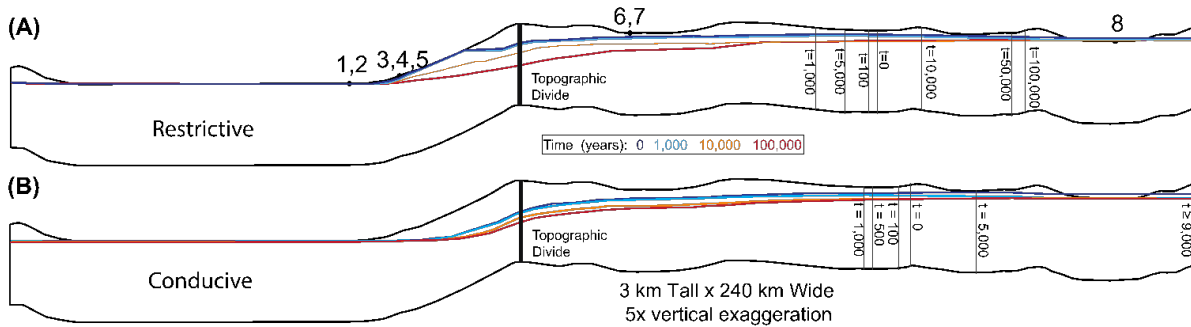


Figure 7: Simulated hydraulic head distributions for (A) restrictive and (B) conductive simulations at time of 0, 1000, 10000, 100000 years after change in recharge. Position of the hydrogeologic divides are shown for labeled times in vertical black lines. Numbered locations correspond to head observations locations plotted in Figure 8.

1260
1261
1262
1263
1264
1265
1266

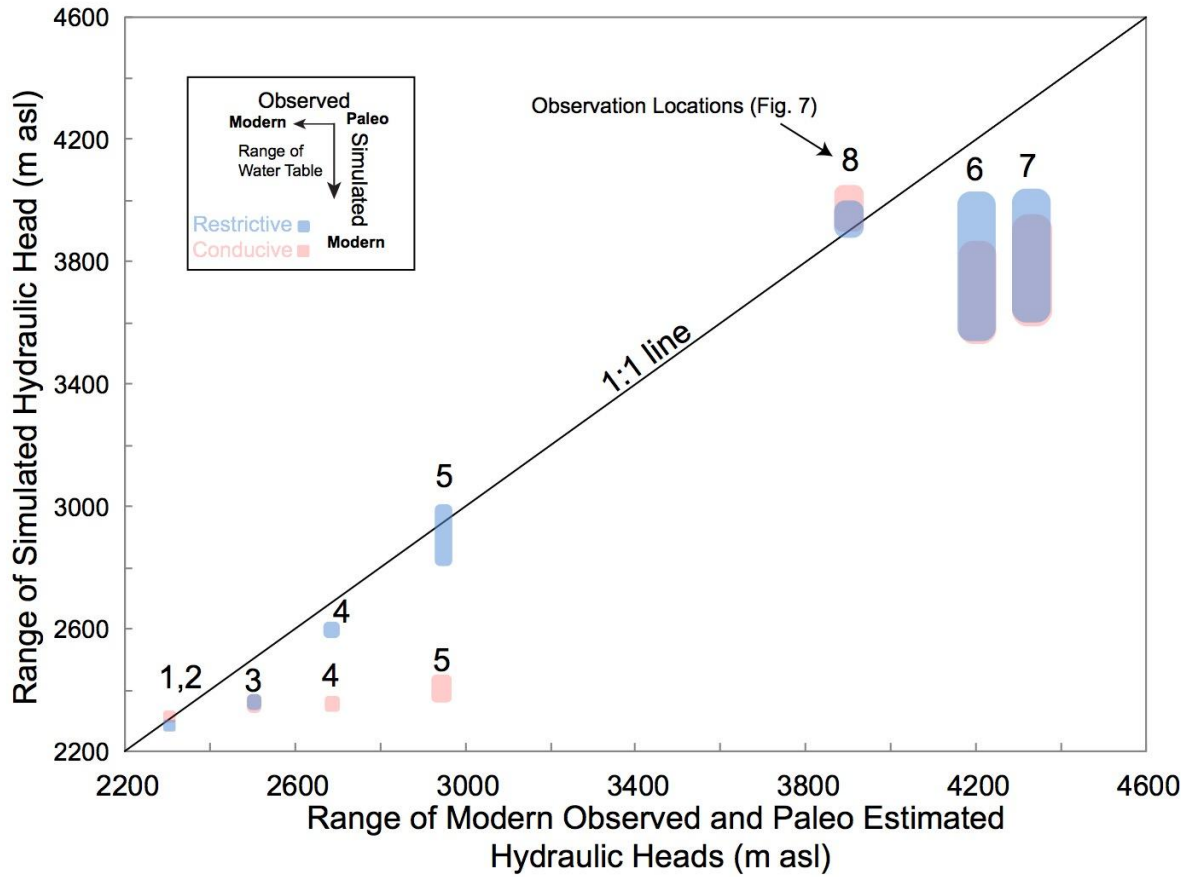


Figure 8 Simulated hydraulic heads (y-axis) for restrictive and conductive simulations compared to modern field and paleo-hydraulic head estimates (x-axis). Sizes of colored polygons (pink – conductive, blue – restrictive) are based on simulated heads with the highest position being the initial condition for the models. Highest observed heads are estimated based on paleo-hydrologic information cited in text and presented in Supporting Information 5.

1267
 1268
 1269
 1270
 1271

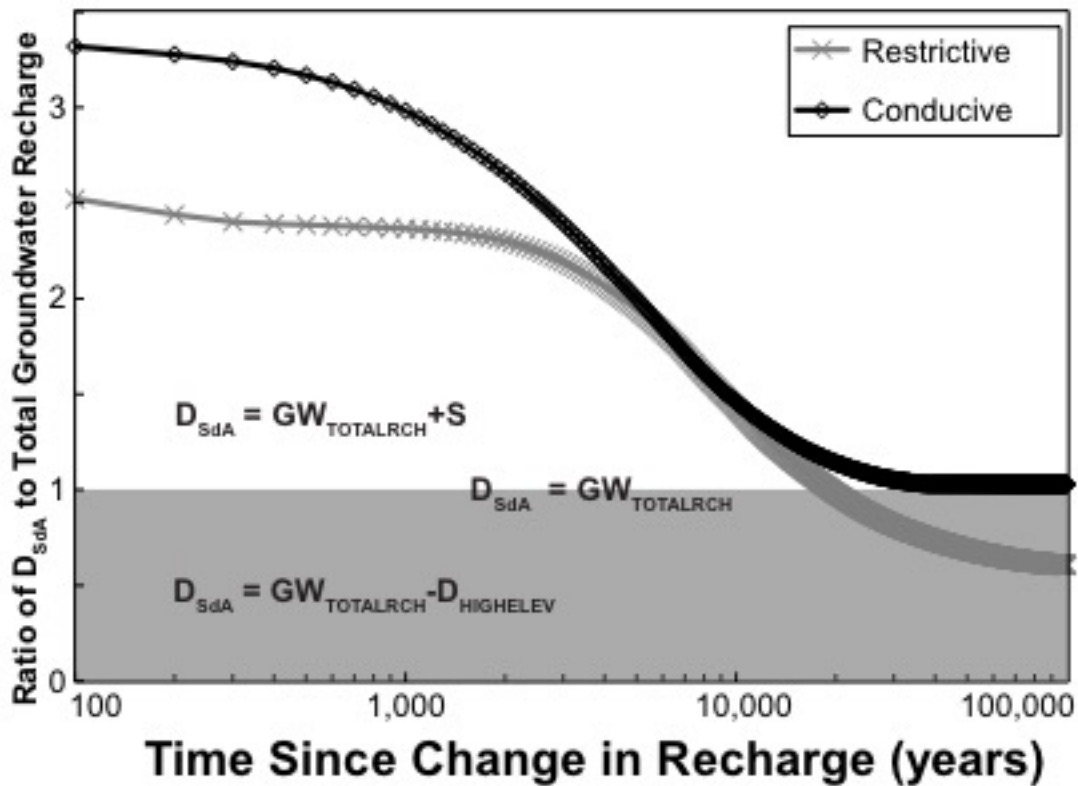
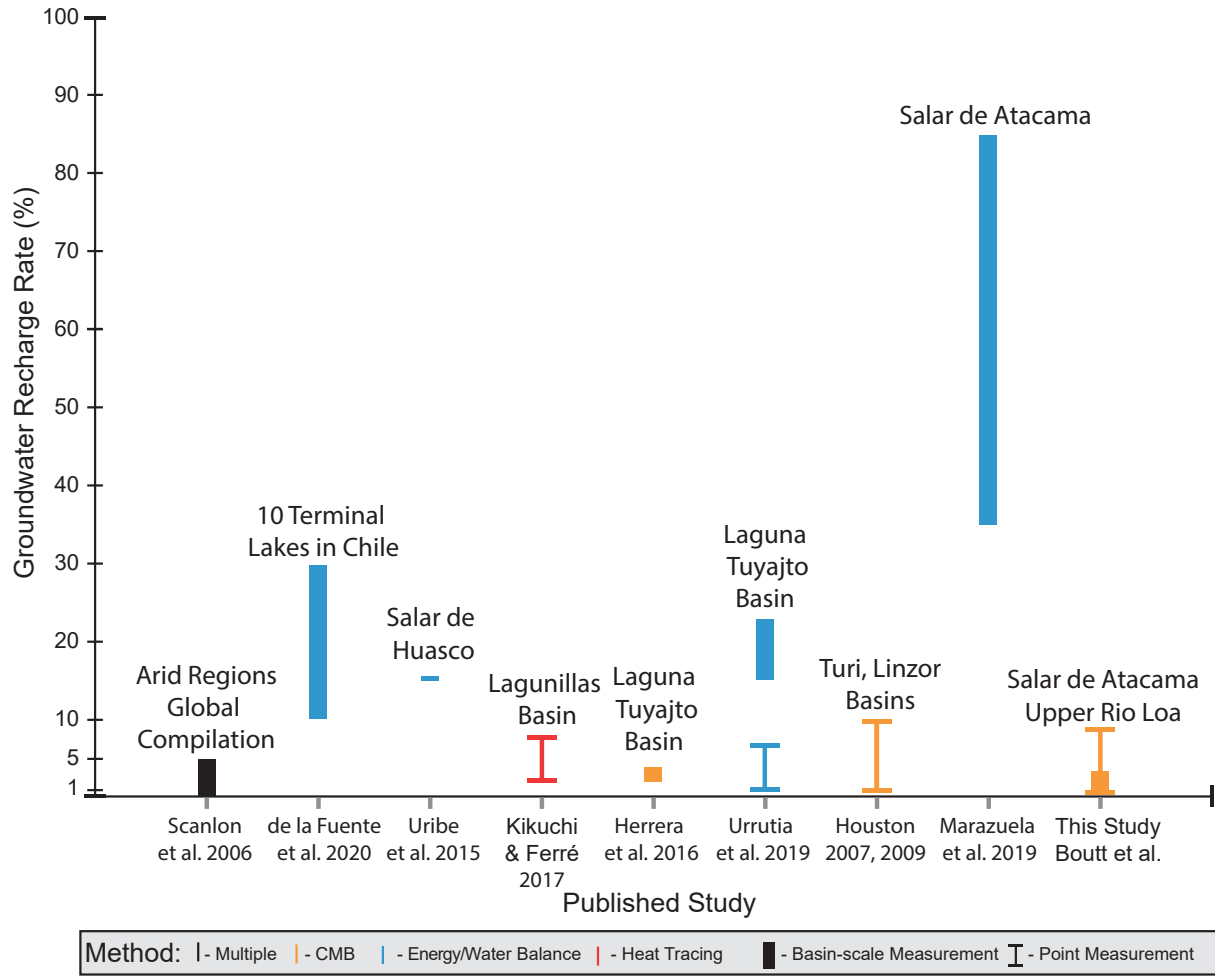


Figure 9 Plot of the ratio of discharge from constant head cells at SdA and drains along the plateau margin (D_{SdA}) to specified total model recharge ($GW_{TOTALRCH}$). The un-shaded region represents discharge to SdA that is greater than total model recharge (i.e. some contribution of groundwater storage). The shaded represents times in the simulation where discharge to SdA is less than the total model recharge.

1272
 1273
 1274
 1275



1276
 1277
 1278
 1279
 1280
 1281
 1282
 1283
 1284
 1285
 1286
 1287
 1288
 1289
 1290
 1291
 1292

Table 1: Locations and characteristics of precipitation samples used to determine chloride concentrations in precipitation

| Sample ID | Date | Longitude | Latitude | Elevation | Cl | $\delta^{18}\text{O}$ | $\delta^2\text{H}$ | Reference |
|------------|-----------|-----------|----------|-----------|----------|-----------------------|--------------------|----------------|
| | | WGS84 | | m asl | mg/ l | ‰ VSMOW | | |
| SDA185W | 41293 | -67.8534 | -23.8374 | 3940 | 9.6 | - 16.9 | -125.7 | N/A |
| SDA190W | 41411 | -68.0673 | -23.6818 | 2381 | 8.1 | - 18.9 | -137.0 | N/A |
| SDA220W | 41655 | -67.8549 | -23.7876 | 3825 | 15.8 | -2.6 | -6.6 | N/A |
| LAC.P001 | 38718 | -67.4450 | -23.8281 | 4307 | <10 | - 18.0 | -135.4 | Cervetto, 2012 |
| Ascotan | 1999-2000 | -68.27 | -21.72 | 3956 | 28 | ND | ND | Houston, 2007 |
| Colchane | 1999-2000 | -68.65 | -19.28 | 3965 | 10 | ND | ND | Houston, 2007 |
| Collacagua | 1999-2000 | -68.83 | -20.05 | 3990 | 4 | ND | ND | Houston, 2007 |
| El Tatio | 1999-2000 | -68 | -22.37 | 4345 | 5 | ND | ND | Houston, 2007 |

1293
1294
1295
1296
1297
1298
1299
1300
1301
1302
1303
1304
1305
1306
1307
1308
1309
1310
1311
1312
1313
1314
1315
1316
1317
1318
1319

Table 2: Predicted Precipitation and Recharge for Topographic and Hydrogeologic Catchments

| | | Topographic | Hydrogeologic Watershed |
|--|-------------------------------|---------------------|-------------------------|
| <i>Total Surface Area (km²)</i> | | 17257 | 75924 |
| <i>Area of Recharge Zones (km²)</i> | | 14319 | 69676 |
| <i>Precipitation</i> | (P) | 30.7 | 199.4 |
| | | (23.4-51.7) | (171.4-284.4) |
| <i>Recharge from precipitation</i> | (GWR) | 1.1 | 10.0 |
| | | (1.1-2.1) | (9.7-14.6) |
| <i>Surface water inflow</i> | (R) | 1.6 | 1.6 |
| | | (0.5-2) | (0.5-2) |
| <i>Evapotranspiration from SdA</i> | (ETSdA) | 9.5 | 9.5 |
| | | (5.6-13.4) | (5.6-13.4) |
| <i>Evapotranspiration from higher elevation salars</i> | (ETHighElevSalars) | 0 | 5.0 |
| | | | (1.8-17.8) |
| ΔStorage | (ΔS) | -6.8 | -2.9 |
| | | (-11.8--1.5) | (-21.0-+9.2) |

1320
1321
1322
1323
1324
1325
1326
1327
1328
1329
1330

1331 Table 3: Tabulated attributes and results of groundwater chloride analyses
1332 including estimates of groundwater recharge from the chloride mass balance
1333 method.

| Site ID | Long. | Lat. | Elev. | Depth to Water | Landscape Position | Potential Recharge Mechanism | Date | Cl _{gw} | Na _{gw} | δ ¹⁸ O | δ ² H | ³ H* p | GWR | GWR/P | |
|-----------|---------|---------|-------|----------------|---|------------------------------|---|--|--|--|---|-------------------|---------------|---------------|---------------|
| SDA139W | -67.988 | -23.495 | 2568 | Spring | Spring at the margin of large canyon | Ephemeral | Average 4/3/12 9/24/12 1/11/13 5/19/13 1/17/14 | 320.9 207.7 201.9 555.3 311.6 327.9 | 222.7 231.8 220.5 225.1 224.0 212.0 | -8.0 -8.3 -7.7 -7.5 -8.1 -8.6 | -56.9 -60.0 -56.8 -54.8 -55.1 -58.0 | 0.14 | 86 | 2.1 (1.3-5.1) | 2.5 (1.6-5.9) |
| SDA140W | -68.050 | -23.476 | 2340 | 18.5 | Well in alluvial fan | Mountain Front Recharge | Average 4/3/12 9/24/12 1/11/13 5/19/13 | 277.3 224.8 366.5 319.9 197.9 | 217.0 210.9 215.6 238.2 203.2 | -8.2 -8.0 -8.4 -8.1 -8.3 | -60.3 -62.4 -63.3 -58.7 -56.6 | 18 | 0.5 (0.3-1.3) | 2.9 (1.8-7.0) | |
| SDA161W | -68.112 | -23.771 | 2338 | 23.4 | Well in stream channel deposit down-gradient of losing perennial stream | Ephemeral | Average 9/29/12 1/12/13 1/13/13 5/14/13 1/14/14 8/18/14 | 1579.7 1650.2 1745.9 1732.7 1949.4 1525.9 873.8 | 913.0 1075.0 904.9 779.4 904.9 1001.9 811.9 | -7.8 -7.6 -7.8 -7.9 -7.8 -8.0 -7.9 | -54.3 -54.6 -54.2 -53.8 -54.2 -55.9 -53.1 | 15 | 0.1 (0-0.2) | 0.5 (0.3-1.0) | |
| SDA186W | -67.985 | -23.491 | 2574 | 21.7 | Well in a alluvial fan deposit | Ephemeral | Average 1/19/13 5/19/13 | 228.5 231.3 225.7 | 215.4 220.1 210.8 | -8.2 -7.9 -8.5 | -58.2 -57.9 -58.5 | 0.11 | 66 | 2.3 (1.4-5.9) | 3.5 (2.2-9.0) |
| SDA226W | -68.137 | -23.794 | 2329 | 13.3 | | Ephemeral | Average 1/19/14 8/18/14 | 1339.9 1457.5 1222.3 | 768.5 811.6 725.5 | -7.3 -7.5 -7.1 | -50.3 -52.2 -48.3 | 17 | 0.1 (0.1-0.2) | 0.6 (0.4-1.2) | |
| SDA227W | -68.134 | -23.800 | 2338 | 25.2 | Well in a alluvial fan deposit down-gradient of MNT | Ephemeral | Average 1/19/14 8/18/14 | 1032.3 842.1 1222.6 | 621.5 686.9 556.1 | -8.7 -8.6 -8.8 | -59.5 -58.0 -60.9 | 17 | 0.1 (0.1-0.3) | 0.8 (0.5-1.6) | |
| SDA228W | -68.136 | -23.789 | 2335 | 11.6 | Well in a alluvial fan deposit down-gradient of MNT | Ephemeral | Average 1/19/14 8/18/14 | 1107.7 948.0 1267.4 | 705.5 711.2 699.8 | -8.8 -9.0 -8.7 | -59.8 -60.8 -58.8 | 17 | 0.1 (0.1-0.3) | 0.7 (0.5-1.5) | |
| SDA229W | -68.118 | -23.746 | 2313 | 4.7 | Well in a alluvial fan deposit down-gradient of MNT | Ephemeral | 1/19/14 | 1232.9 | 882.3 | -8.8 | -61.1 | 17 | 0.1 (0.1-0.2) | 0.6 (0.4-1.4) | |
| SDA2W | -68.081 | -23.671 | 2333 | 15 | Well in the alluvial fan downgradient localized spring discharge site | Ephemeral | Average 9/30/11 1/12/12 4/8/12 9/26/12 | 1328.4 1983.3 1097.1 1414.2 819.0 | 782.6 696.2 718.6 798.8 916.8 | -7.3 -7.7 -8.7 -8.6 -8.6 | -52.2 -56.2 -63.4 -65.6 -61.2 | 0.11 | 28 | 0.2 (0.1-0.4) | 0.6 (0.4-1.3) |
| SDA76W | -68.053 | -23.365 | 2387 | 43.6 | Well in a alluvial fan deposit | Mountain Front Recharge | Average 1/13/12 4/3/12 1/11/13 5/19/13 | 369.0 354.2 370.6 382.9 368.4 | 340.3 301.1 365.1 341.9 353.1 | -7.3 -7.3 -7.5 -7.1 -7.4 | -52.2 -52.2 -54.7 -51.3 -50.5 | 0.15 | 18 | 0.4 (0.2-0.9) | 2.2 (1.4-5.0) |
| SDA84W | -68.057 | -23.569 | 2329 | 9.9 | Well in channel deposit down-gradient of losing perennial stream | Ephemeral | Average 1/14/12 4/7/12 9/24/12 5/19/13 1/11/13 1/9/14 | 2309.2 2214.0 2830.9 2197.2 2042.3 2259.0 2312.0 | 1460.1 1446.5 1620.1 1334.5 1284.0 1722.3 1353.2 | -8.2 -8.3 -8.2 -8.2 -7.9 -8.2 -8.3 | -58.4 -59.3 -60.5 -59.6 -56.2 -56.2 -58.7 | 0.47 | 14 | 0.0 (0-0.1) | 0.3 (0.2-0.7) |
| SDA85W | -68.114 | -23.780 | 2351 | 23.1 | Well in channel deposit down-gradient of losing perennial stream | Ephemeral | Average 1/14/12 4/8/12 9/25/12 1/12/13 5/14/13 1/9/14 | 1632.6 1527.8 1867.5 1576.7 1668.3 1483.7 1671.4 | 958.5 921.6 1048.1 1000.4 957.3 852.0 971.4 | -8.3 -8.3 -8.3 -8.4 -8.2 -8.2 -8.3 | -59.2 -60.5 -62.5 -62.4 -57.6 -55.8 -56.5 | 15 | 0.1 (0-0.2) | 0.5 (0.3-1.0) | |
| SDA8AW | -68.109 | -23.791 | 2373 | Spring | Perennial spring fed stream at base of large discharge | Ephemeral | 1/9/14 | 1323.1 | 867.0 | -9.2 | -64.2 | 0.10 ^g | 17 | 0.1 (0.1-0.2) | 0.6 (0.4-1.3) |
| COL.T008 | -67.507 | -23.885 | 4261 | No Data | High altitude swale | Diffuse | Average 10/30/08 10/30/08 | 960.0 994.3 925.6 | 652.0 692.0 612.0 | -11.3 -11.2 -11.4 | -81.1 -81.2 -80.9 | 90 | 0.8 (0.5-1.6) | 0.9 (0.5-1.8) | |
| PN.T005.1 | -67.451 | -23.676 | 4376 | 31.1 | High altitude swale | Diffuse | Average 11/26/04 11/26/04 11/27/04 | 1220.0 1250.0 1220.0 1190.0 | 0.0 0.0 0.0 0.0 | -11.0 -11.0 -10.9 -11.1 | -81.5 -80.2 -81.4 -82.9 | 44 | 0.3 (0.2-0.6) | 0.7 (0.4-1.4) | |
| PN.T006.1 | -67.451 | -23.693 | 4364 | 44.4 | High altitude swale | Diffuse | 11/27/04 | 1220.0 | 0.0 | -11.1 | -82.0 | 44 | 0.3 (0.2-0.6) | 0.7 (0.4-1.4) | |
| PN.T007.6 | -67.452 | -23.692 | 4361 | No Data | High altitude swale | Diffuse | Average 9/1/05 1/16/05 1/20/05 | 1533.3 1510.0 1540.0 1530.0 | 593.3 593.0 597.0 590.0 | -11.2 -11.2 -11.2 -11.2 | -81.7 -79.8 -82.8 -82.5 | 44 | 0.2 (0.1-0.5) | 0.5 (0.3-1.1) | |
| PN.T008.2 | -67.453 | -23.677 | 4374 | 52.89 | High altitude swale | Diffuse | Average 12/22/04 1/16/05 1/20/05 | 1250.0 1260.0 1240.0 1250.0 | 434.7 425.0 442.0 437.0 | -11.1 -11.2 -11.2 -11.0 | -81.8 -81.4 -82.0 -81.9 | 44 | 0.3 (0.2-0.6) | 0.6 (0.4-1.3) | |
| PN.T014 | -67.449 | -23.678 | 4383 | No Data | High altitude swale | Diffuse | 10/29/08 | 1097.1 | 0.0 | -11.1 | -81.7 | 44 | 0.3 (0.2-0.7) | 0.7 (0.5-1.5) | |

Supporting Information

Imbalance in the modern hydrologic budget of topographic catchments along the western slope of the Andes (21–25°S): Implications for groundwater recharge assessment

David F. Boutt¹, Lilly G. Coenthall¹, Brendan J. Moran¹, LeeAnn Munk², Scott A.

Hynek³,

¹ Department of Geosciences, University of Massachusetts-Amherst, Amherst, MA, USA

² Department of Geological Sciences, University of Alaska-Anchorage, Anchorage, AK, USA

³Department of Geology and Geophysics, University of Utah, Salt Lake City, Utah USA

Contents of this file

Text S1 to S5

Figures S1 to S4

Tables S1 to S6

Text S1.

Calculation of Median, Lower and Upper Precipitation Bounds. To incorporate uncertainty into our analysis of precipitation in the regional precipitation dataset we consider 3 instances of precipitation estimates. The median precipitation value is the processed TRMM 2B31 dataset from [Bookhagen and Strecker, 2008], which has already been evaluated against gauge data in the region and is shown to be a good estimate of precipitation. To evaluate the bias of TRMM 2B31 in this region we can compare the satellite estimates against station data from Direccion General de Aguas (DGA) (Figure S1) in Figure S2. Specific station data are provided in Table 1. While the fit between the remote sensed and station data is very good, we consider two different scenarios for estimating precipitation bias. In each case, we modify the magnitude of the spatial distribution of precipitation using the TRMM data to calculate both a lower and upper bound precipitation values. A power law is fit to the data in the region of the greatest misfit (< 75 mm/yr) in the TRMM dataset. Functions fit to the lower and upper bounds are used to calculate a modified precipitation map and for the corresponding water balance calculations. For both bounds for values greater than 75 mm/yr we simply revert back to the TRMM 2B31 data. These estimates capture more than a 100% of variation in precipitation estimates.

Text S2.

Expanded Evapotranspiration Estimates Methods

This equation, whereby $PET[mm] = 4367[m] - (0.59 * \text{ground elevation}[m])$, was developed by Houston [2006a] based on pan evaporation from 12 meteorological stations. This equation was applied to a 30 m² resolution Advanced Spaceborne Thermal Emission and Reflection Radiometer (ASTER) Global Digital Elevation Model (GDEM) to calculate gridded PET for the region. Polygons outlining the borders of fresh lakes and salars were manually constructed based on Landsat imagery, and estimates of PET were applied to permanent zones of discharge (salar and fresh lakes). The mean PET (mm/year) for each polygon (m²) is used to derive an estimated PET from each high elevation salar or lake (m³/s) (Figure S3 and Tables S2 and S3). To determine the actual evapotranspiration (AET) we compare our PET estimates to published AET estimates for SdA [Mardones, 1986; Kampf and Tyler, 2006] and Salar de Pedernales [Johnson et al., 2010]. Mean annual AET is approximately 2% of PET for the lower D_{SdA} estimate (5.6 m³/s) and the Salar de Pedernales, and 8% of the upper D_{SdA} estimate (22.7 m³/s). Conservatively, we therefore consider that AET could vary from 0.5 to 8% of PET for

salars in the region depending on depth to water table and other factors. We assume that AET is 80% of PET for Miniques and Miscanti Lakes (specific conductance between 7,780 and 10,640 $\mu\text{S}/\text{cm}$).

Text S3.

Evaluation of the impact of Chloride Concentration in Precipitation and Precipitation magnitude on Chloride Mass Balance Recharge Calculations. Inspecting equation 3 in the manuscript it demonstrates that both total precipitation and the chloride concentration have a positive impact on the predicated amount of groundwater recharge. Additionally, setting the term Cl_{rw} (chloride from rock weathering) to zero we also can increase the groundwater recharge. Here, we consider the sources of uncertainty in the derived precipitation-recharge relationship in the chloride mass balance method using the median precipitation (described in S1) and an average chloride concentration of 8 mg/L and the upper precipitation bound and a high chloride concentration (16 mg/L) with no contribution of Cl from rock weathering. The resulting precipitation-recharge estimates calculated for our groundwater samples described in the text is depicted in Figure S5 along with a power law fit to the data. The estimated precipitation-recharge amounts, for observed chloride concentrations in both groundwater and precipitation fall along a distribution that is well fit by a single power law. Therefore, in the manuscript we use a single power-law to calculate recharge amounts from precipitation scenarios.

Text S4.

Groundwater Footprint and Water Table Ratio. The groundwater footprint [Gleeson *et al.*, 2012] of SdA, considering only non-anthropogenic discharge, is 5–21 times larger than the topographic watershed (Text S4, Figure S6, and Table S5), which ranks among the largest footprints of aquifers studied in the world. This is especially significant since the calculations of Gleeson *et al.* (2012) are based predominantly on anthropogenic discharge rates. The discharge to recharge ratio (Qr:R; [Schaller and Fan, 2009]), a metric of whether a basin is a groundwater importer or exporter, indicates the topographic watershed, with a Qr:R ratio of 4.9–19.9, is a strong importer of groundwater. Modern shallow groundwater and surface water inflow to SdA reasonably balance low estimates of evapotranspiration; however, modern GW_{RCH} within the topographic watershed alone cannot explain the magnitude of these fluxes. We modify the groundwater footprint calculation [Gleeson *et al.*, 2012], to include groundwater abstraction only from natural sources (evapotranspiration) in order to approximate the area required to support discharge rates. The groundwater footprint (GF) can be described according to Gleeson *et al.* [2012] by $\text{GF} = A[\text{ET}/(\text{GWR}-\text{R})]$, where A is the area of interest, ET is the groundwater abstraction rate, GWR is the recharge rate and R is baseflow. For the SdA topographic watershed, we calculate a groundwater footprint of 87,850-365,121 km^2 , or 5-21 times the area of the topographic watershed. The range is based using median GWR and the upper and lower ranges of reasonable ET estimates.

We calculate the water table ratio (WTR) for the topographic watershed of SdA following methods outlined in Haitjema and Mitchell Bruker [2005] and Gleeson *et al.* [2011]. The WTR is a dimensionless criterion that describes whether the water table is likely (1) topographically controlled where the water table follows topography, or (2) recharge controlled where the water

table is disconnected from topography and there is strong potential for inter-basin flow. The WTR is defined by $\log \log (WTR) = \log \left(\frac{RL^2}{mKHd} \right)$, with abbreviations explained in *Gleeson et al.*, [2011], where a more positive $\log(WTR)$ suggests topography controlled water tables and a more negative $\log(WTR)$ suggests recharge controlled water tables. We estimate a range of $\log(WTR)$ for the watershed from -3.6 to -5.3, which suggests a strongly recharge-controlled water table similar to those of the arid southwestern United States [*Gleeson et al.*, 2012].

Text S5.

Dynamic Response Time Calculations. The residence time of a system is equated to its response time using a simple box model of an aquifer system to calculate the e-folding time, or the time to readjust to new boundary conditions. The above residence time estimate does not take into account the dynamics of the hydraulic response of the system (i.e. how changes in hydraulic head are propagated from the plateau to the basin). The dynamic response time (τ_{DRes}) of a 1-dimensional homogenous aquifer can be

approximated as $\tau_{DRes} = \frac{L^2}{D} = \frac{L^2 S}{bK}$, where L is a characteristic length of the flow system

(here taken as the maximum length of a flow path), $D = \frac{Kb}{S}$ is the hydraulic diffusivity, K is the hydraulic conductivity, b is the aquifer thickness (here assumed to be 500 m) and S is the aquifer storage coefficient.

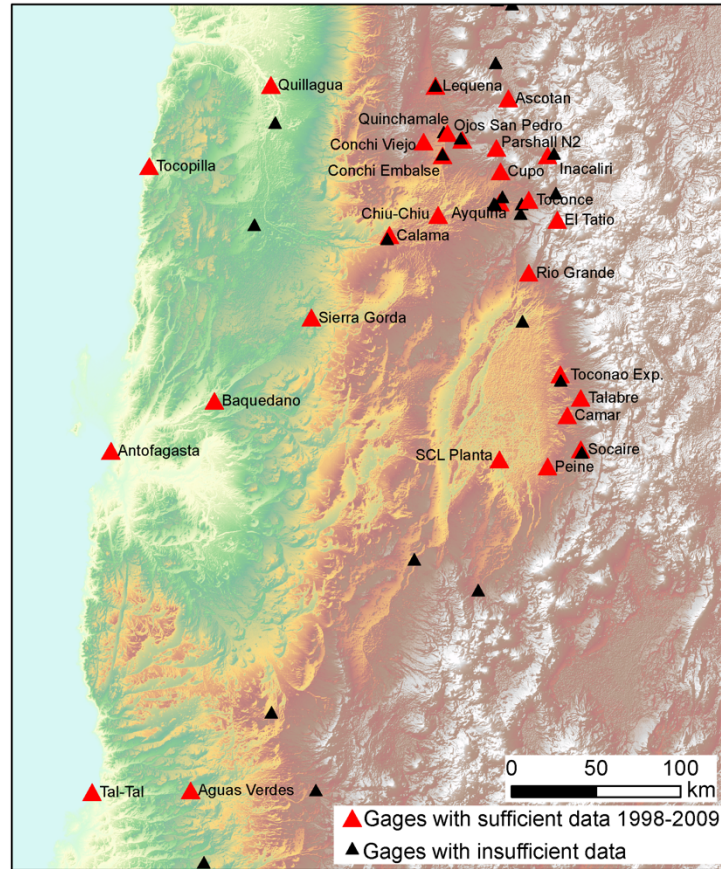


Figure S1. Meteorological stations in the Region of Antofagasta, Chile with sufficient data from the period of 1998-2009 (red triangles) and stations with discontinuous or discontinued measurements (black triangles). All stations are maintained by the Chilean Government’s Direccion General de Aguas (DGA), with the exception of SCL Planta that has been maintained by the Sociedad Chilena de Litio/Rockwood Lithium, Inc/Albermarle.

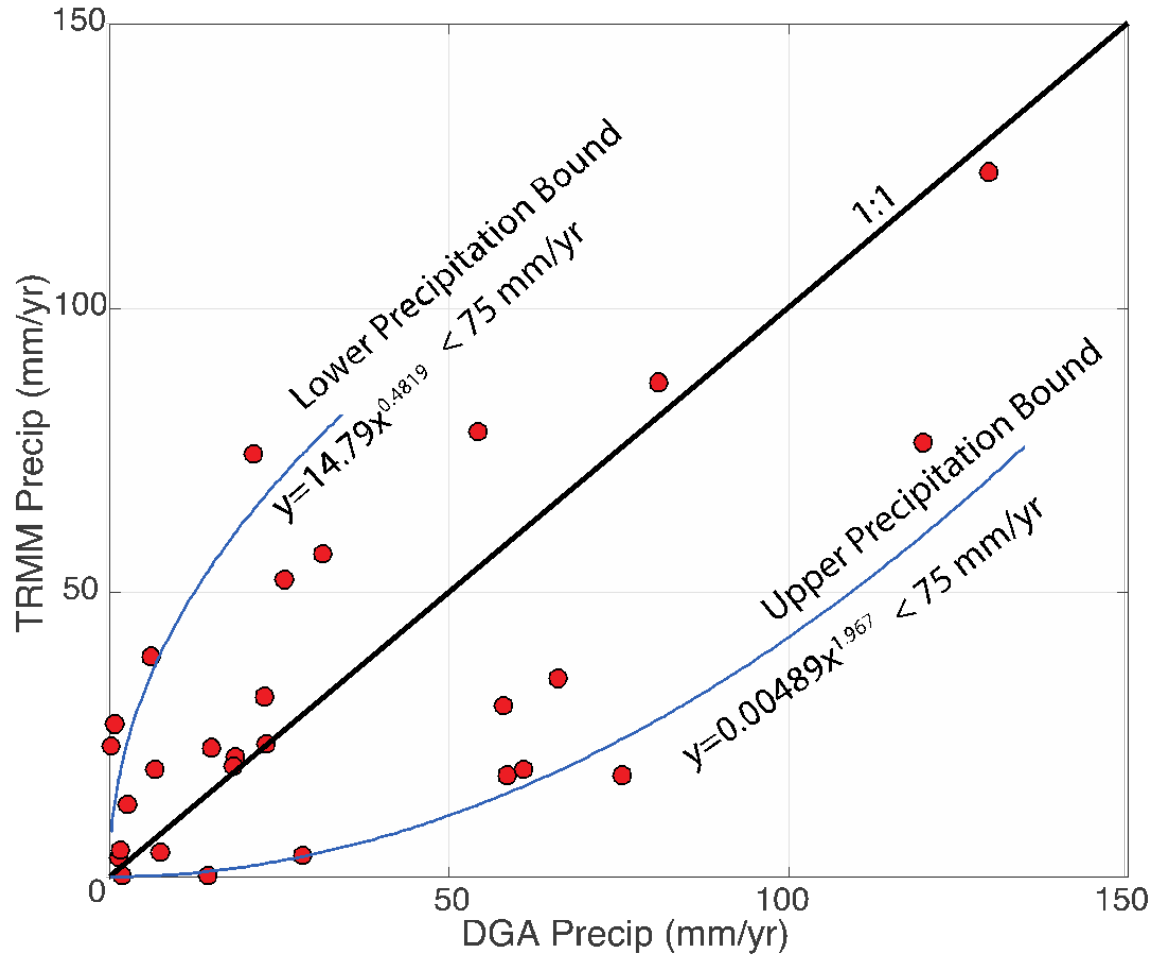


Figure S2. Comparison of gage data with remotely sensed precipitation estimates. Average annual precipitation from 1998-2009 calculated from monthly DGA raw measurements (<http://snia.dga.cl/BNAConsultas/reportes>) and one measurement from the Sociedad Chilena de Lito/Rockwood Lithium Inc. meteorological station. TRMM 2B31 estimate of precipitation from the TRMM 2B31 dataset [Bookhagen and Strecker, 2008] for sites in the Region of Antofagasta, Chile. Power functions are fit to calculate lower and upper bound precipitation maps for water balance calculations.

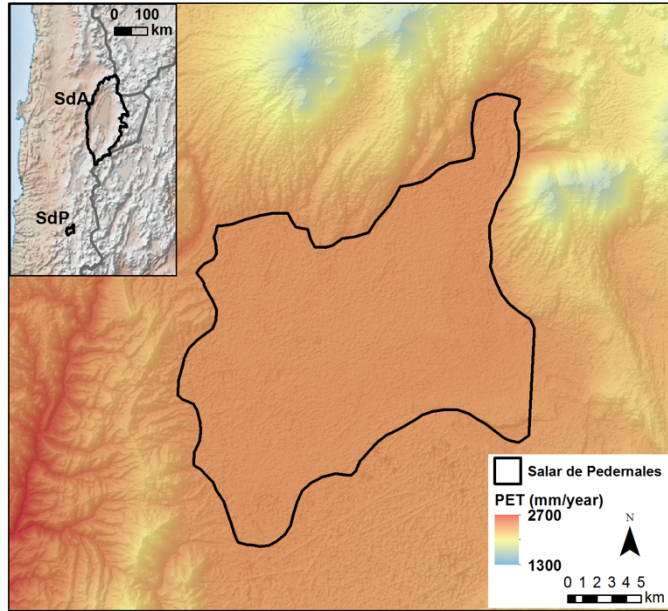


Figure S3. Map of PET computed by equation (a) in the Salar de Pedernales (SdP) region. Background is an ASTER DEM. SdP border modified from *Johnson et al.* [2010]. The SdP has a surface area of 315 km², average elevation of 3356 m asl and average PET of 2384 mm/year (standard deviation of 6 mm/year).

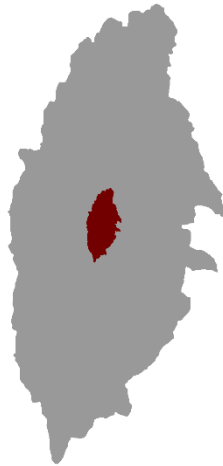


Figure S4. Conservative groundwater footprint of the SdA topographic watershed. The red zone is the topographic watershed area, and the gray shaded region is its inferred groundwater footprint based on a groundwater discharge rate of 5.6 m³/s.

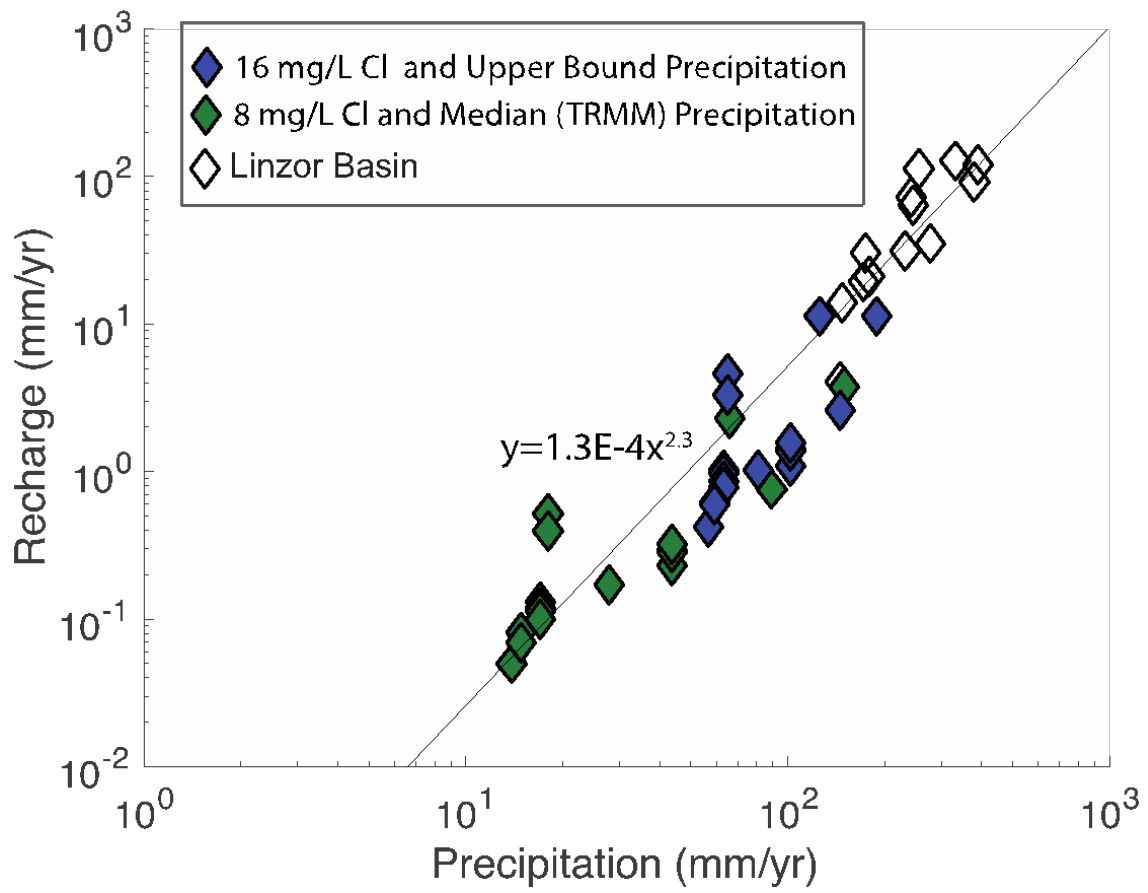


Figure S5. Precipitation-Recharge Relationship from Chloride Mass Balance Calculations.

| Meteorological Station | Easting | Northing | Elevation | Distance from SdA | Precipitation | |
|------------------------|---------|----------|-----------|-------------------|---------------|-----------|
| | | | | | Gage | TRMM 2B31 |
| | WGS84 | | m asl | km | mm/year | mm/year |
| Aguas Verdes | 403389 | 7190650 | 1600 | 270 | 6.7 | 18.7 |
| Antofagasta | 358725 | 7389982 | 50 | 220 | 2 | 0.2 |
| Ascotan | 575136 | 7597754 | 3956 | 200 | 66.2 | 34.9 |
| Ayquina | 570227 | 7536538 | 3031 | 140 | 31.4 | 56.6 |
| Baquadano | 414749 | 7419946 | 1032 | 160 | 1.5 | 4.6 |
| Calama | 509841 | 7517409 | 2260 | 130 | 2.8 | 12.7 |
| Camar | 606276 | 7411224 | 3020 | 30 | 25.9 | 52.3 |
| Chiu-Chiu | 536440 | 7529250 | 2524 | 140 | 6.3 | 38.7 |
| Conchi Embalse | 539003 | 7564490 | 3010 | 170 | 14.5 | 0.1 |
| Conchi Viejo | 528514 | 7572609 | 3491 | 180 | 28.6 | 3.7 |
| Cupo | 570641 | 7554915 | 3600 | 160 | 81 | 86.8 |
| El Tatio | 601729 | 7526160 | 4320 | 130 | 129.7 | 123.7 |
| Inacaliri | 596588 | 7564208 | 4100 | 170 | 119.8 | 76.4 |
| Lequena | 535139 | 7605268 | 3320 | 210 | 61 | 18.7 |
| Ojos San Pedro | 568440 | 7568716 | 3800 | 170 | 58 | 30.0 |
| Parshall N2 | 549805 | 7573477 | 3318 | 180 | 23.1 | 23.1 |
| Peine | 595346 | 7381030 | 2480 | 20 | 18.6 | 20.9 |
| Quillagua | 444822 | 7605629 | 802 | 250 | 0.4 | 23.0 |
| Quinchamale | 541684 | 7577572 | 3020 | 180 | 18.3 | 19.6 |
| Rio Grande | 585833 | 7495117 | 3250 | 100 | 58.7 | 17.9 |
| SCL Plant | 569278 | 7385349 | 2300 | 0 | 15.1 | 22.7 |
| Sierra Gorda | 467247 | 7468888 | 1616 | 130 | 0.9 | 26.8 |
| Socaire | 613485 | 7391129 | 3251 | 40 | 22.8 | 31.7 |
| Talabre | 613735 | 7421435 | 3600 | 40 | 54.4 | 78.1 |
| Tal-Tal | 350886 | 7189130 | 9 | 310 | 7.5 | 4.4 |
| Toconao Exp. | 602581 | 7435191 | 2430 | 40 | 21.3 | 74.3 |
| Toconce | 586111 | 7537991 | 3350 | 140 | 75.6 | 17.9 |
| Tocopilla | 378070 | 7557678 | 45 | 250 | 1.3 | 3.4 |

Table S1. Comparison of average annual precipitation between gage and remotely sensed sources from 1998-2009 from DGA gage measurements (<http://snia.dga.cl/BNAConsultas/reportes>) and one measurement from the Sociedad Chilena de Litio meteorological station (SCL Planta) with gridded precipitation from the TRMM 2B31 dataset [Bookhagen and Strecker, 2008] for the Region of Antofagasta, Chile.

| Salar | Surface Area km ² | Average Elevation m asl | AET m ³ /s | Mean PET mm/year | Standard Deviation mm/year | Mean PET m ³ /s | AET/PET % | Reference for AET estimate |
|---------------------|--|-----------------------------------|---------------------------------|----------------------------|--------------------------------------|--------------------------------------|---------------------|-----------------------------------|
| Salar de Atacama | 2750 | 2313 | 5.6 | 2999 | 13 | 262 | 2 | Mardones, 1986 / DGA, 2010 |
| | 2864 | 2313 | 22.7 | 2999 | 13 | 272 | 8 | Kampf and Tyler, 2006 |
| Salar de Pedernales | 315 | 3356 | 0.58 | 2384 | 6 | 24 | 2 | Johnson et al., 2010 |

Table S2. Actual evapotranspiration as a fraction of potential evapotranspiration derivation for the Salar de Pedernales and Salar de Atacama.

| Zone | Area (km ²) | Mean PET (m ³ /s) | Mean AET (m ³ /s) | | | Zone | Area (km ²) | Mean PET (m ³ /s) | Mean AET (m ³ /s) | | | |
|-------|----------------------------|---------------------------------|------------------------------|---------|---------|---------|----------------------------|---------------------------------|------------------------------|---------|---------|---------|
| | | | 2% | 0.5% | 8% | | | | 2% | 0.5% | 8% | |
| B | 1.3* | 8.2E-02 | 6.5E-02 | 6.5E-02 | 6.5E-02 | J | 3.3 | 1.8E-01 | 3.6E-03 | 9.0E-04 | 1.4E-02 | |
| | 12.8* | 7.8E-01 | 6.2E-01 | 6.2E-01 | 6.2E-01 | | 1.2 | 6.4E-02 | 1.3E-03 | 3.2E-04 | 5.1E-03 | |
| | 1.8 | 1.0E-01 | 2.0E-03 | 5.1E-04 | 8.2E-03 | | 34.1 | 1.9E+00 | 3.7E-02 | 9.3E-03 | 1.5E-01 | |
| C | 112.6 | 6.7E+00 | 1.3E-01 | 3.4E-02 | 5.4E-01 | | 22.9 | 1.2E+00 | 2.5E-02 | 6.1E-03 | 9.8E-02 | |
| | 13.3 | 7.2E-01 | 1.4E-02 | 3.6E-03 | 5.8E-02 | | 4.9 | 2.6E-01 | 5.3E-03 | 1.3E-03 | 2.1E-02 | |
| | 14.9 | 8.6E-01 | 1.7E-02 | 4.3E-03 | 6.9E-02 | | 6.9 | 3.8E-01 | 7.6E-03 | 1.9E-03 | 3.0E-02 | |
| D | 11.8 | 7.7E-01 | 1.5E-02 | 3.8E-03 | 6.1E-02 | | 1.8 | 1.0E-01 | 2.0E-03 | 5.0E-04 | 8.0E-03 | |
| | 22.2 | 1.4E+00 | 2.9E-02 | 7.2E-03 | 1.2E-01 | | 33.5 | 1.9E+00 | 3.7E-02 | 9.3E-03 | 1.5E-01 | |
| | 13.5 | 8.8E-01 | 1.8E-02 | 4.4E-03 | 7.0E-02 | | K | 81.0 | 5.3E+00 | 1.1E-01 | 2.6E-02 | 4.2E-01 |
| | 29.6 | 2.1E+00 | 4.2E-02 | 1.1E-02 | 1.7E-01 | | | 19.1 | 1.3E+00 | 2.5E-02 | 6.3E-03 | 1.0E-01 |
| E | 3.0 | 2.2E-01 | 4.3E-03 | 1.1E-03 | 1.7E-02 | 141.5 | 9.3E+00 | 1.9E-01 | 4.6E-02 | 7.4E-01 | | |
| | 1.9 | 1.1E-01 | 2.3E-03 | 5.7E-04 | 9.1E-03 | 2.1 | 1.1E-01 | 2.3E-03 | 5.7E-04 | 9.1E-03 | | |
| F | 2.6 | 1.6E-01 | 3.3E-03 | 8.2E-04 | 1.3E-02 | 1.9 | 1.0E-01 | 2.0E-03 | 5.1E-04 | 8.1E-03 | | |
| | 11.9 | 8.7E-01 | 1.7E-02 | 4.4E-03 | 7.0E-02 | 2.1 | 1.1E-01 | 2.3E-03 | 5.7E-04 | 9.2E-03 | | |
| | 15.5 | 9.2E-01 | 1.8E-02 | 4.6E-03 | 7.3E-02 | L | 113.2 | 8.3E+00 | 1.7E-01 | 4.2E-02 | 6.7E-01 | |
| G | 8.3 | 4.9E-01 | 9.9E-03 | 2.5E-03 | 3.9E-02 | | 1091.5 | 8.0E+01 | 1.6E+00 | 4.0E-01 | 6.4E+00 | |
| | 71.4 | 4.3E+00 | 8.6E-02 | 2.1E-02 | 3.4E-01 | | 154.0 | 1.1E+01 | 2.2E-01 | 5.4E-02 | 8.6E-01 | |
| | 39.2 | 2.3E+00 | 4.5E-02 | 1.1E-02 | 1.8E-01 | | 12.1 | 7.6E-01 | 1.5E-02 | 3.8E-03 | 6.1E-02 | |
| | 0.6 | 3.2E-02 | 6.4E-04 | 1.6E-04 | 2.6E-03 | | 20.8 | 1.4E+00 | 2.9E-02 | 7.2E-03 | 1.1E-01 | |
| | 1.3 | 6.4E-02 | 1.3E-03 | 3.2E-04 | 5.2E-03 | M | 119.4 | 8.3E+00 | 1.7E-01 | 4.2E-02 | 6.7E-01 | |
| 1.2 | 6.2E-02 | 1.2E-03 | 3.1E-04 | 5.0E-03 | 5.4 | | 2.9E-01 | 5.7E-03 | 1.4E-03 | 2.3E-02 | | |
| 105.0 | 5.9E+00 | 1.2E-01 | 3.0E-02 | 4.7E-01 | 12.8 | | 6.9E-01 | 1.4E-02 | 3.4E-03 | 5.5E-02 | | |
| H | 58.1 | 4.8E+00 | 9.6E-02 | 2.4E-02 | 3.8E-01 | | 115.7 | 6.4E+00 | 1.3E-01 | 3.2E-02 | 5.1E-01 | |
| | 51.8 | 3.0E+00 | 6.0E-02 | 1.5E-02 | 2.4E-01 | 1.0 | 5.2E-02 | 1.0E-03 | 2.6E-04 | 4.2E-03 | | |
| | 0.9 | 5.0E-02 | 1.0E-03 | 2.5E-04 | 4.0E-03 | 2.9 | 1.6E-01 | 3.2E-03 | 8.0E-04 | 1.3E-02 | | |
| | 2.8 | 1.5E-01 | 3.0E-03 | 7.6E-04 | 1.2E-02 | 0.8 | 4.7E-02 | 9.4E-04 | 2.3E-04 | 3.8E-03 | | |
| | 0.6 | 3.2E-02 | 6.4E-04 | 1.6E-04 | 2.5E-03 | 1.5 | 8.2E-02 | 1.6E-03 | 4.1E-04 | 6.5E-03 | | |
| | 1.8 | 9.4E-02 | 1.9E-03 | 4.7E-04 | 7.5E-03 | 3.7 | 2.1E-01 | 4.2E-03 | 1.0E-03 | 1.7E-02 | | |
| | 16.9 | 9.1E-01 | 1.8E-02 | 4.5E-03 | 7.3E-02 | 5.4 | 3.0E-01 | 6.1E-03 | 1.5E-03 | 2.4E-02 | | |
| | 1.9 | 1.0E-01 | 2.0E-03 | 5.0E-04 | 8.0E-03 | N | 247.5 | 2.1E+01 | 4.1E-01 | 1.0E-01 | 1.6E+00 | |
| | 0.2 | 1.1E-02 | 2.2E-04 | 5.5E-05 | 8.8E-04 | | 19.9 | 1.4E+00 | 2.8E-02 | 7.0E-03 | 1.1E-01 | |
| | 5.2 | 3.0E-01 | 6.0E-03 | 1.5E-03 | 2.4E-02 | | 7.3 | 4.3E-01 | 8.6E-03 | 2.2E-03 | 3.4E-02 | |
| 15.3 | 9.5E-01 | 1.9E-02 | 4.8E-03 | 7.6E-02 | 0.5 | | 3.1E-02 | 6.1E-04 | 1.5E-04 | 2.5E-03 | | |
| 7.3 | 3.7E-01 | 7.5E-03 | 1.9E-03 | 3.0E-02 | 98.6 | | 7.1E+00 | 1.4E-01 | 3.6E-02 | 5.7E-01 | | |
| 358.8 | 2.5E+01 | 4.9E-01 | 1.2E-01 | 2.0E+00 | 24.4 | 1.6E+00 | 3.2E-02 | 7.9E-03 | 1.3E-01 | | | |
| J | 120.5 | 8.2E+00 | 1.6E-01 | 4.1E-02 | 6.6E-01 | O | 144.9 | 9.8E+00 | 2.0E-01 | 4.9E-02 | 7.9E-01 | |
| | 0.4 | 2.2E-02 | 4.3E-04 | 1.1E-04 | 1.7E-03 | | 0.6 | 3.4E-02 | 6.8E-04 | 1.7E-04 | 2.7E-03 | |
| | 2.2 | 1.1E-01 | 2.2E-03 | 5.6E-04 | 9.0E-03 | | 0.8 | 4.1E-02 | 8.2E-04 | 2.1E-04 | 3.3E-03 | |
| | 0.9 | 4.7E-02 | 9.3E-04 | 2.3E-04 | 3.7E-03 | | 2.5 | 1.4E-01 | 2.7E-03 | 6.8E-04 | 1.1E-02 | |
| | 0.8 | 4.0E-02 | 7.9E-04 | 2.0E-04 | 3.2E-03 | | 0.6 | 3.3E-02 | 6.6E-04 | 1.7E-04 | 2.7E-03 | |
| | 12.5 | 6.9E-01 | 1.4E-02 | 3.5E-03 | 5.5E-02 | | | | | | | |

Table S3. Summary of land type, surface area, mean annual potential evapotranspiration (PET) and actual evapotranspiration (AET) for the discharge zone polygons in all considered watersheds. Each lettered watershed includes all cumulative discharge zones in the smaller watersheds. Starred areas in watershed B are Miscanti and Miniquest lakes where AET is assumed to be 80 % of PET.

| Variable | Abbreviation | Value |
|---|---------------------|-------------------|
| Surface area (km ²) | A | 17,257 |
| Discharge (m ³ /s) | ET | 5.6 to 22.7 |
| Recharge (m ³ /s) | GWR | 1.1 |
| Baseflow contribution (m ³ /s) | R | 0 |
| Groundwater Footprint (km ²) | GF | 87,850 to 356,120 |
| Groundwater stress indicator | GF/A | 5 to 21 |

Table S4. Groundwater footprint calculations for the SdA topographic watershed. Values are specific to SdA and variables and calculations described in *Gleeson et al.* [2012]. Discharge estimates from Mardones [1986] and *Kampf and Tyler* [2006]. We consider an R of 0 consistent with the more conservative water budget conceptualization.

| Description | Abbreviation | Value |
|--|---------------------|--------------|
| Areal recharge rate (mm/year) | R | 2.5 |
| Distance between surface water bodies (km) | L | 10 |
| Hydraulic conductivity (m/day) | K | 1 to 10 |
| Average vertical extent of groundwater flow system (m) | H | 100 to 500 |
| Maximum terrain rise (m) | d | 3700 |
| Constant (unitless) | m | 8 |
| log Water Table Ratio | log(WTR) | -3.6 to -5.3 |

Table S5. Water Table Ratio for the SdA topographic watershed. The average areal recharge rate is calculated based on the raster of GWR presented in Figure 3b, and the maximum terrain rise is derived from an ASTER DEM. Values approximate bulk aquifer properties for the SdA. We copy the values presented in *Gleeson et al.* [2011] for distance between surface water bodies, and more conservative estimate for the average vertical extent of the flow system.

| Observation Point ID | Hydraulic Head Constraints (masl) | | Simulated initial heads (masl) | | Total change in head over simulation (m) | | Reference for Hydraulic Head Constraints | Notes |
|----------------------|-----------------------------------|-------|--------------------------------|-----------------|--|------------|---|---|
| | Modern | Paleo | Restrictive Case | Conductive Case | Restrictive | Conductive | | |
| 1 | 2309 | 2314 | 2311 | 2315 | <1 | <1 | Field Measured Water Levels | Paleo Head of +5 m is estimated based on position relative to Tulan Wetlands |
| 2 | 2310 | 2315 | 2311 | 2315 | 5 | 5 | Field Measured Water Levels | Paleo Head of +5 m is estimated based on position relative to Tulan Wetlands |
| 3 | 2498 | 2509 | 2335 | 2328 | 20 | 10 | Betancourt et al., 2000 - Tulan Wetlands | Rio Tulan deposits showed a rise of ~11 m above current levels between 8.2 and 3.0 ky BP. Observed heads based on approximate location of modern spring discharge |
| 4 | 2692 | 2702 | 2602 | 2345 | 25 | 15 | Betancourt et al., 2000 - Taranje Wetlands | Taranje paleowetland deposits are at a higher elevation than the Tulan deposits. Taranje deposits date between 15.4 and 9.0 ky BP. Observed heads based on approximate location of modern spring discharge |
| 5 | 2960 | 2975 | 2964 | 2390 | 180 | 25 | Springs at Imilac and Punta Negra Quade et al 2008 - Midpoint ground elevation between the Salar de Imilac (2970 m asl) & Salar de Punta Negra (2950 m asl) | SdI & SdP are south of SdA, so approximate elevations are projected onto a similar elevation on east side (where the model geometry was derived), note that Imilac springs are fault controlled according to Quade, Observed heads based on approximate location of modern spring discharge |
| 6 | 4210 | 4240 | 3980 | 3842 | 460 | 350 | Cervetto (2012) Wells - LA and LAAR wells, Grosjean et al., 1995 | Water Elevations in LA and LAAR series wells from Anexo G of Cervetto's thesis range from 4208-4216m, Laguna Tuyajito estimates of +20-40 m |
| 7 | 4320 | 4345 | 4005 | 3916 | 460 | 350 | Cervetto (2012) Wells - PN and PNAR wells, Grosjean et al., 1995 | Water Elevations in PN series wells from Anexo G of Cervetto's thesis range from 4320-4322m, Aguas Calientes IV +25 m |
| 8 | 3900 | 4000 | 3993 | 4008 | 100 | 100 | Modern Levels - Salar de Olaroz Ground elevation is 3900m (https://www.orocobre.com/PDF/NI%2043-101_Technical%20Report-Oloroz%20Project.pdf) | Paleo high stands of ~ 100 m (Grosjean et al., 1995, Placzek et al., 2006, 2013) |

Table S6. Simulation results and estimates of modern and paleo hydraulic heads for specific places within the model domain. Sources of estimates and notes discussing them in 2 right-hand columns of table.